

A Lagrangian Perturbation Theory in the presence of massive neutrinos

Alejandro Aviles^{a,b} Arka Banerjee^{c,d,e}

^aConsejo Nacional de Ciencia y Tecnología, Av. Insurgentes Sur 1582, Colonia Crédito Constructor, Del. Benito Jurez, 03940, Ciudad de México, México

^bDepartamento de Física, Instituto Nacional de Investigaciones Nucleares, Apartado Postal 18-1027, Col. Escandón, Ciudad de México, 11801, México.

^cKavli Institute for Particle Astrophysics and Cosmology, Stanford University, 452 Lomita Mall, Stanford, CA 94305, USA

^dDepartment of Physics, Stanford University, 382 Via Pueblo Mall, Stanford, CA 94305, USA

^eSLAC National Accelerator Laboratory, 2575 Sand Hill Road, Menlo Park, CA 94025, USA

E-mail: avilescervantes@gmail.com, arkab@stanford.edu

Abstract. We develop a Lagrangian Perturbation Theory (LPT) framework to study the clustering of cold dark matter (CDM) in cosmologies with massive neutrinos. We follow the trajectories of CDM particles with Lagrangian displacements fields up to third order in perturbation theory. Once the neutrinos become non-relativistic, their density fluctuations are modeled as being proportional to the CDM density fluctuations, with a scale-dependent proportionality factor. This yields a gravitational back-reaction that introduces additional scales to the linear growth function, which is accounted for in the higher order LPT kernels. Through non-linear mappings from Eulerian to Lagrangian frames, we ensure that our theory has a well behaved large scale behavior free of unwanted UV divergences, which are common when neutrino and CDM densities are not treated on an equal footing, and in resummation schemes that manifestly break Galilean invariance. We use our theory to construct correlation functions for both the underlying matter field, as well as for biased tracers using Convolution-LPT. Redshift-space distortions effects are modeled using the Gaussian Streaming Model. When comparing our analytical results to simulated data from the QUIJOTE¹ simulation suite, we find good accuracy down to $r = 20 \text{ Mpc } h^{-1}$ at redshift $z = 0.5$, for the real space and redshift space monopole particle correlation functions with no free parameters. The same accuracy is reached for the redshift space quadrupole if we additionally consider an effective field theory parameter that shifts the pairwise velocity dispersion. For modeling the correlation functions of tracers we adopt a simple Lagrangian biasing scheme with only density and curvature operators, which we find sufficient to reach down to $r = 20 \text{ Mpc } h^{-1}$ when comparing to simulated halos.

Keywords: Large Scale Structure, Massive neutrinos, Perturbation Theory

¹<https://github.com/franciscovillaescusa/Quijote-simulations>

Contents

1	Introduction	1
2	Lagrangian displacements	4
3	Perturbation Theory	7
3.1	2LPT	7
3.2	Third order Lagrangian displacements	9
4	Neutrino density	11
5	Real space correlation function	16
6	Redshift-space correlation function	19
7	Results for halos	23
8	Summary and Conclusions	27
A	k- and q-functions	29

1 Introduction

Relic neutrinos produced in the early Universe are the second most abundant standard model particles. Hence, despite their tiny masses, their contribution to the total cosmological density budget at low redshifts is non-negligible. Neutrino oscillation experiments give lower bounds for the sum of their masses, being 0.06 eV for a normal hierarchy and 0.11 eV for inverted hierarchy [1]. On the other hand measurements of the Cosmic Microwave Background (CMB) anisotropies from the Planck satellite yield an upper bound of 0.24 eV. This tightens to 0.12 eV when combined with BAO observations [2], with strong degeneracies with H_0 and σ_8 . While the lower mass bounds on neutrino mass imply that massive neutrinos relevant for structure formation must be non-relativistic at late times, the thermal velocities of the neutrinos are still relevant down to $z = 0$, since they decoupled from the primordial plasma while still relativistic. The thermal velocity introduces a new scale in the problem - the free streaming scale [3]. On scales larger than the free-streaming scale, the neutrino thermal velocity is not large enough to prevent gravitational collapse into the potential wells set by CDM and baryons, but on smaller scales, the thermal velocities prevent the growth of the neutrino perturbations. For realistic neutrino masses, this scale is $\sim 100 \text{ Mpc } h^{-1}$. The other relevant scale is the maximum value of the free streaming scale over the history of the Universe's evolution. On scales larger than this, neutrinos, once they are non-relativistic, and CDM behave exactly the same. On scales smaller than this scale, the neutrino power spectrum is damped with respect to the CDM power spectrum. For realistic neutrino masses, this scale is $\sim 1 \text{ Gpc } h^{-1}$. Since the growth of the neutrino perturbations on small scales is prevented by the presence of large thermal velocities, the total matter power spectrum, which includes terms arising from the CDM-neutrino cross spectrum and the neutrino power spectrum, are damped compared to a massless neutrino cosmology. The CDM power spectrum is

itself also damped compared to a massless neutrino cosmology. This is due to the fact that the neutrinos contribute to the source term of the Poisson equation that drives the growth of the CDM perturbations. The damping of both the CDM power spectrum, and the total matter power spectrum scale with the neutrino mass, with a different prefactor for each [3].

Ongoing and future galaxy surveys, such as eBOSS¹, DESI², Euclid³ and LSST⁴, will impose tighter constraints on the sum of the neutrino masses and potentially detect their mass ordering [4–8]. As the redshift depth and angular size of galaxy surveys increase, they cover scales where quasi-linear effects are more relevant and the tools of Perturbation Theory (PT) become even more important [9]. To fully exploit the forthcoming wealth of data using analytical and semi-analytical methods, comprehensive theories of clustering, valid on these quasi-linear scales, are needed. The construction of such models has been widely developed within the massless neutrinos Λ CDM. However, for cosmologies that include the effects of massive neutrinos the situation is rather different, and comparatively less work on the subject has been produced so far. Moreover, almost all studies in PT beyond linear order have focused on Fourier space [10–21], so non-linear analytical tools for computing the real and redshift space correlation functions are still lacking in the literature; but see, e.g., [22], where the authors study the degradation and shift of the BAO peak by using the resummation theory of [23] with Einstein-de Sitter (EdS) kernels. In [24] a 2LPT theory that treats neutrinos as linear is constructed for using it in a hybrid N -body/PT, COLA scheme.

On the other hand, advances in simulation methods have ensured that the effects of massive neutrinos can now be included in N -body simulations of structure formation, at the level of accuracy needed for the future surveys. While numerous different techniques have been adopted for this purpose [25–32], their results mostly agree on the quasi-linear scales of interest in this paper. These simulations, therefore, provide an ideal test-bed for calibrating analytic and semi-analytic models of real-space clustering. Once the latter has been tested against measurements from simulations, they can be used over a wide range of cosmological parameter space without having to run computationally expensive simulations.

In this work we construct a Lagrangian Perturbation Theory (LPT) for cold dark matter clustering in the presence of massive neutrinos, accounting for the additional scale dependence introduced by the free-streaming. The presence of non-negligible thermal velocities of neutrinos is an added complication for the Lagrangian approach to structure formation in cosmology. For CDM particles, all particles starting at initial coordinate \mathbf{q} follow the same trajectory $\mathbf{x}(t)$ as a function of time, and coherent flows are found for patches of a few Mpc. This leads to a sensible definition of the displacement field, which is the object of interest for Lagrangian approaches. Neutrino particles, on the other hand, have very different trajectories as a function of time, even if they start at the same position, due to differences in the magnitude and direction of their thermal velocities.⁵ This leads to difficulties in defining a single-valued displacement field which captures the correct evolution of neutrino particles—in [34, 35] this problem is overcome for the simpler case of a single warm dark matter fluid. For this reason in this work Lagrangian displacements will follow the trajectories of CDM

¹<https://www.sdss.org/surveys/eboss/>

²<https://www.desi.lbl.gov/>

³<https://sci.esa.int/web/euclid>

⁴<https://www.lsst.org/>

⁵This complication is also present in the Eulerian approach since it is not possible to have a well defined velocity field at small scales, and needs to be addressed directly with the Boltzmann equation, as in [21]. Other works approximate the neutrinos as a perfect fluid with a Jeans-like mechanism with Jeans length settled by the free-streaming scale [17, 33].

particles, and non-linear neutrinos overdensities, once non-relativistic, will be approximated to be proportional to the CDM fluctuations, where both are equal at scales much larger than the free-streaming, while damped by a factor equal to the ratio of their linear densities at smaller scales. Since we will assume adiabatic perturbations throughout, this factor is given by the ratio of the transfer functions of neutrinos and CDM. This approach is analogous to some studies in the Eulerian framework [13, 15], where it is shown that this approximation introduces an error of $\sim 0.1\%$.

With the Lagrangian displacement kernels at hand, we construct the 2-point statistics for the density and velocity fields to 1-loop order in PT. We do this to obtain the real space correlation function using the formalism of Convolution-LPT (CLPT) [36], and the redshift space correlation function using the Gaussian Streaming Model (GSM) [37, 38], with the pairwise velocity and velocity dispersion computed with CLPT. Since the presence of the free-streaming introduces further scale-dependencies into the LPT kernels, the way to obtain the ingredients of the GSM differs from the massless neutrino Λ CDM model; for this endeavour we will use the formalism recently developed in [39] in the context of modified gravity.

We test our theory against data obtained from the QUIJOTE simulations suite [40] for neutrinos with total mass $M_\nu = \sum_i m_{\nu,i} = 0, 0.1, 0.2$ and 0.4 eV at redshift $z = 0.5$, where the masses are distributed equally among the three mass eigenstates. We find that our formalism is capable of accurately fitting the simulation measurements (for particles) of the real space and redshift-space monopole correlation functions down to $20 \text{ Mpc } h^{-1}$ with no free parameters, while the redshift-space quadrupole shows the same level of accuracy only if we add an additional Effective Field Theory (EFT) parameter that serves to shift significantly the pairwise velocity dispersion [37, 41]. For halos with masses $13.1 < \log_{10} [M_h / (M_\odot h^{-1})] < 13.5$, we are capable to reach down to $20 \text{ Mpc } h^{-1}$ with the use of linear and second order Lagrangian local biases, and a curvature bias. However, we note that the latter is only necessary when the bias is defined with respect to the total correlation function (i.e. including both CDM and neutrino components), while being consistent with zero when the bias is defined with respect to the CDM correlation function (with the exception of the case $M_\nu = 0.4 \text{ eV}$). This agrees with previous studies that show that linear bias, although scale-dependent in the presence of massive neutrinos, can be well approximated by a (time-dependent) constant when the biasing prescription is applied to the CDM component only, but not when it is applied to the total matter field [42–46].

The rest of this work is organized as follows. The general formalism is presented in section 2, arriving at the evolution equation for the CDM Lagrangian displacement field in eq. (2.24). In section 3 we find the kernels of the Lagrangian displacement up to third order in PT, given in eqs. (3.4), (3.8) and (3.18). In section 4 we discuss our approximation for the neutrino density field and how this leads to a well behaved theory free of UV divergences. We construct the real space and redshift space correlation functions in sections 5 and 6 where we also compare to CDM and CDM + neutrino particle simulated data. In section 7 we test our formalism against CDM halos. Finally in section 8 we present our conclusions. Some calculations are presented in Appendix A.

2 Lagrangian displacements

The trajectories $\mathbf{x}(t)$ of cold dark matter particles are related to their initial, Lagrangian positions \mathbf{q} as

$$\mathbf{x}(t) = \mathbf{q} + \Psi(\mathbf{q}, t), \quad (2.1)$$

where $\Psi(\mathbf{q}, t)$ is the Lagrangian displacement vector field, assumed longitudinal and initially Gaussian distributed. Henceforth, we will omit the time argument, and assume implicitly that they are functions of time. Using mass conservation one can relate the Lagrangian displacement to the overdensity

$$\delta_{cb}(\mathbf{x}) = \frac{1 - J(\mathbf{q})}{J(\mathbf{q})}. \quad (2.2)$$

Following a standard notation in the literature, subscript “ cb ” means that we are referring to the combined CDM-baryons fluid, although we will treat the baryons as CDM particles. $J_{ij}(\mathbf{q}) = \delta_{ij} + \Psi_{i,j}(\mathbf{q})$ is the Jacobian matrix of the coordinates transformation (2.1) and J its determinant. The geodesic equation yields

$$\nabla_{\mathbf{x}} \cdot \hat{\mathcal{T}}\Psi(\mathbf{q}) = -\frac{1}{a^2} \nabla_{\mathbf{x}}^2 \Phi(\mathbf{x}), \quad (2.3)$$

with Φ the Newtonian potential. We use $\nabla_{\mathbf{x}} = \partial/\partial\mathbf{x}$ to denote partial derivatives with respect to Eulerian coordinates. A comma is used to denote differentiation with respect to Lagrangian coordinates. We further define the linear operator [47]

$$\hat{\mathcal{T}} = \frac{d^2}{dt^2} + 2H \frac{d}{dt}, \quad (2.4)$$

and for notational compactness we introduce

$$A_0 = 4\pi G \bar{\rho}_m. \quad (2.5)$$

In (q -)Fourier space

$$[\nabla_{\mathbf{x}} \cdot \hat{\mathcal{T}}\Psi(\mathbf{q})](\mathbf{k}) = -A_0 f_{cb} \tilde{\delta}_{cb}(\mathbf{k}) - \tilde{S}(\mathbf{k}), \quad (2.6)$$

with $f_{cb} \equiv \Omega_{cb}/\Omega_m$, and $[(\dots)](\mathbf{k})$ indicates the Fourier transform of $(\dots)(\mathbf{q})$. We have used the Poisson equation

$$\frac{1}{a^2} \nabla_{\mathbf{x}}^2 \Phi(\mathbf{x}) = A_0 f_{cb} \tilde{\delta}_{cb}(\mathbf{k}) + \tilde{S}(\mathbf{k}). \quad (2.7)$$

In general, we do not write a tilde over Fourier transforms, but we do it in $\tilde{\delta}_{cb}(\mathbf{k})$ and $\tilde{S}(\mathbf{k})$ to emphasize that they are q -Fourier transform of their Eulerian position counterparts; that is, for a general function $f(\mathbf{x})$,

$$\tilde{f}(\mathbf{k}) = \int \frac{d^3k}{(2\pi)^3} e^{i\mathbf{k}\cdot\mathbf{q}} f(\mathbf{x}). \quad (2.8)$$

The source term $\tilde{S}(\mathbf{k})$ is the neutrino density

$$\tilde{S}(\mathbf{k}) = A_0 f_{\nu} \tilde{\delta}_{\nu}(\mathbf{k}) \equiv A_0 f_{\nu} \tilde{\alpha}(\mathbf{k}) \tilde{\delta}_{cb}(\mathbf{k}), \quad (2.9)$$

where $f_{\nu} \equiv \Omega_{\nu}/\Omega_m = 1 - f_{cb}$, and in the last equality we have introduced the function $\tilde{\alpha}(\mathbf{k}) \equiv \tilde{\delta}_{\nu}/\tilde{\delta}_{cb} = \tilde{\alpha}(k)$, where the angular dependencies $\hat{\mathbf{k}}$ cancel since they are carried by

the primordial initial conditions set down by inflation. Later we will discuss more about this function α . For the moment we will treat \tilde{S} as a source proportional to the cb density perturbations. Our strategy is to write the rhs of eq. (2.6) in terms of only Lagrangian coordinates. For the CDM density field, eq. (2.2) implies

$$-\tilde{\delta}_{cb}(\mathbf{k}) = \left[\Psi_{i,i} - \frac{1}{2}((\Psi_{i,i})^2 + \Psi_{i,j}\Psi_{j,i}) + \frac{1}{6}(\Psi_{i,i})^3 + \frac{1}{3}\Psi_{i,j}\Psi_{j,k}\Psi_{k,i} - \frac{1}{2}\Psi_{k,k}\Psi_{i,j}\Psi_{j,i} + \dots \right](\mathbf{k}), \quad (2.10)$$

where we stop at cubic powers of the Lagrangian displacement. We need now to write the factor $\tilde{\alpha}(\mathbf{k})$ of the source \tilde{S} in Lagrangian coordinates. We expand a general function $f(\mathbf{x})$ around $\mathbf{x} = \mathbf{q}$, $f(\mathbf{x}) = f(\mathbf{q} + \Psi) = f(\mathbf{q}) + \Psi_i(\mathbf{q})f_{,i}(\mathbf{q}) + \frac{1}{2}\Psi_i(\mathbf{q})\Psi_j(\mathbf{q})f_{,ij}(\mathbf{q}) + \dots$, and with the use of eq. (2.8) this implies the following relation between x - and q -Fourier transforms⁶

$$\begin{aligned} \tilde{f}(\mathbf{k}) &= f(\mathbf{k}) + \int_{\mathbf{k}_{12}=\mathbf{k}} h_i^{ff}(\mathbf{k}_1, \mathbf{k}_2) f(\mathbf{k}_1) \Psi_i(\mathbf{k}_2) \\ &+ \int_{\mathbf{k}_{123}=\mathbf{k}} h_{ij}^{ff}(\mathbf{k}_1, \mathbf{k}_2, \mathbf{k}_3) f(\mathbf{k}_1) \Psi_i(\mathbf{k}_2) \Psi_j(\mathbf{k}_3) + \dots, \end{aligned} \quad (2.13)$$

and the inverse relation

$$\begin{aligned} f(\mathbf{k}) &= \tilde{f}(\mathbf{k}) + \int_{\mathbf{k}_{12}=\mathbf{k}} h_i^{\tilde{f}f}(\mathbf{k}_1, \mathbf{k}_2) \tilde{f}(\mathbf{k}_1) \Psi_i(\mathbf{k}_2) \\ &+ \int_{\mathbf{k}_{123}=\mathbf{k}} h_{ij}^{\tilde{f}f}(\mathbf{k}_1, \mathbf{k}_2, \mathbf{k}_3) \tilde{f}(\mathbf{k}_1) \Psi_i(\mathbf{k}_2) \Psi_j(\mathbf{k}_3) + \dots, \end{aligned} \quad (2.14)$$

with

$$h_i^{ff}(\mathbf{k}_1, \mathbf{k}_2) = -h_i^{\tilde{f}f}(\mathbf{k}_1, \mathbf{k}_2) = ik_1^i, \quad (2.15)$$

$$h_{ij}^{ff}(\mathbf{k}_1, \mathbf{k}_2, \mathbf{k}_3) = -\frac{1}{2}k_1^i k_1^j, \quad (2.16)$$

$$h_{ij}^{\tilde{f}f}(\mathbf{k}_1, \mathbf{k}_2, \mathbf{k}_3) = -h_{ij}^{ff}(\mathbf{k}_1, \mathbf{k}_2, \mathbf{k}_3) + h_i^{ff}(\mathbf{k}_{13}, \mathbf{k}_2) h_j^{\tilde{f}f}(\mathbf{k}_1, \mathbf{k}_3). \quad (2.17)$$

We use eqs. (2.13) and (2.14) to transform $\tilde{\alpha}$ to α , yielding

$$\begin{aligned} -\frac{1}{A_0 f_\nu} \tilde{S}(\mathbf{k}) &= -\alpha(\mathbf{k}) \tilde{\delta}_{cb}(\mathbf{k}) - \int_{\mathbf{k}_{12}=\mathbf{k}} (\alpha(\mathbf{k}_1) - \alpha(\mathbf{k})) h_i^{ff}(\mathbf{k}_1, \mathbf{k}_2) \tilde{\delta}_{cb}(\mathbf{k}_1) \Psi_i(\mathbf{k}_2) \\ &- \int_{\mathbf{k}_{123}=\mathbf{k}} \left\{ \alpha(\mathbf{k}) h_{ij}^{\tilde{f}f}(\mathbf{k}_1, \mathbf{k}_2, \mathbf{k}_3) + \alpha(\mathbf{k}_{13}) h_i^{ff}(\mathbf{k}_{13}, \mathbf{k}_2) h_j^{\tilde{f}f}(\mathbf{k}_1, \mathbf{k}_3) \right. \\ &\quad \left. + \alpha(\mathbf{k}_1) h_{ij}^{\tilde{f}f}(\mathbf{k}_1, \mathbf{k}_2, \mathbf{k}_3) \right\} \tilde{\delta}_{cb}(\mathbf{k}_1) \Psi_i(\mathbf{k}_2) \Psi_j(\mathbf{k}_3). \end{aligned} \quad (2.18)$$

⁶Throughout we use the shorthand notations

$$\mathbf{k}_{1\dots n} = \mathbf{k}_1 + \dots + \mathbf{k}_n, \quad (2.11)$$

and

$$\int_{\mathbf{k}_{1\dots n}=\mathbf{k}} = \int \frac{d^3 k_1 \dots d^3 k_n}{(2\pi)^{3n}} (2\pi)^3 \delta_D(\mathbf{k}_{1\dots n} - \mathbf{k}). \quad (2.12)$$

Now, using eq. (2.10) in the cb overdensities inside the convolution integrals of the above equation, we can write

$$\begin{aligned} -\tilde{S}(\mathbf{k}) = & -A_0 f_\nu \alpha(\mathbf{k}) \tilde{\delta}_{cb}(\mathbf{k}) - \int_{\mathbf{k}_{12}=\mathbf{k}} \mathcal{K}_{ki}^{\text{FL}\Psi}(\mathbf{k}_1, \mathbf{k}_2) \Psi_k(\mathbf{k}_1) \Psi_i(\mathbf{k}_2) \\ & - \int_{\mathbf{k}_{123}=\mathbf{k}} \mathcal{K}_{kij}^{\text{FL}\Psi}(\mathbf{k}_1, \mathbf{k}_2, \mathbf{k}_3) \Psi_k(\mathbf{k}_1) \Psi_i(\mathbf{k}_2) \Psi_j(\mathbf{k}_3), \end{aligned} \quad (2.19)$$

with

$$\mathcal{K}_{ki}^{\text{FL}\Psi}(\mathbf{k}_1, \mathbf{k}_2) = A_0 f_\nu (\alpha(\mathbf{k}_1) - \alpha(\mathbf{k})) k_1^k k_1^i, \quad (2.20)$$

$$\begin{aligned} \mathcal{K}_{kij}^{\text{FL}\Psi}(\mathbf{k}_1, \mathbf{k}_2, \mathbf{k}_3) = & -i A_0 f_\nu (\alpha(\mathbf{k}) - \alpha(\mathbf{k}_1)) k_1^k k_1^i k_1^j \\ & + i A_0 f_\nu (\alpha(\mathbf{k}) - \alpha(\mathbf{k}_{13})) (k_1^i + k_3^i) \left[k_1^j k_1^k + \frac{1}{2} k_1^k k_3^j + \frac{1}{2} k_1^j k_3^k \right]. \end{aligned} \quad (2.21)$$

We will refer to the terms that contain the kernels $\mathcal{K}_{ij\dots}^{\text{FL}\Psi}$ as “frame-lagging”, since they arise when mapping Fourier transforms between Eulerian and Lagrangian frames. These terms are necessary in LPT frameworks beyond Λ CDM with additional scales defined in Eulerian coordinates. They were used first in [48] in the context Modified Gravity (MG), in a different, less general method we have followed here, and later in other MG works [49–52] and for a COLA implementation with MG and massive neutrinos [24].

Now, introducing the function

$$A(k) = A_0 [f_{cb} + f_\nu \alpha(k)], \quad (2.22)$$

eq. (2.6) becomes

$$\begin{aligned} [\nabla_{\mathbf{x}} \cdot \hat{\mathcal{T}}\Psi](\mathbf{k}) = & -A(k) \tilde{\delta}_{cb}(\mathbf{k}) - \int_{\mathbf{k}_{12}=\mathbf{k}} \mathcal{K}_{ki}^{\text{FL}\Psi}(\mathbf{k}_1, \mathbf{k}_2) \Psi_k(\mathbf{k}_1) \Psi_i(\mathbf{k}_2) \\ & - \int_{\mathbf{k}_{123}=\mathbf{k}} \mathcal{K}_{kij}^{\text{FL}\Psi}(\mathbf{k}_1, \mathbf{k}_2, \mathbf{k}_3) \Psi_k(\mathbf{k}_1) \Psi_i(\mathbf{k}_2) \Psi_j(\mathbf{k}_3). \end{aligned} \quad (2.23)$$

Using $\nabla_{\mathbf{x}} \cdot \hat{\mathcal{T}}\Psi = (J^{-1})_{ij} \hat{\mathcal{T}}\Psi_{i,j} = \hat{\mathcal{T}}\Psi_{i,i} - \Psi_{i,j} \hat{\mathcal{T}}\Psi_{i,j} + \Psi_{i,k} \Psi_{k,j} \hat{\mathcal{T}}\Psi_{i,j} + \dots$ and eq. (2.10) we arrive at the equation of motion for the displacement field

$$\begin{aligned} (\hat{\mathcal{T}} - A(k))[\Psi_{i,i}](\mathbf{k}) = & [\Psi_{i,j} \hat{\mathcal{T}}\Psi_{j,i}](\mathbf{k}) - \frac{A(k)}{2} [\Psi_{i,j} \Psi_{j,i}](\mathbf{k}) - \frac{A(k)}{2} [(\Psi_{l,l})^2](\mathbf{k}) \\ & - [\Psi_{i,k} \Psi_{k,j} \hat{\mathcal{T}}\Psi_{j,i}](\mathbf{k}) + \frac{A(k)}{6} [(\Psi_{l,l})^3](\mathbf{k}) + \frac{A(k)}{2} [\Psi_{l,l} \Psi_{i,j} \Psi_{j,i}](\mathbf{k}) + \frac{A(k)}{3} [\Psi_{i,k} \Psi_{k,j} \Psi_{j,i}](\mathbf{k}) \\ & - \int_{\mathbf{k}_{12}=\mathbf{k}} \mathcal{K}_{ki}^{\text{FL}\Psi}(\mathbf{k}_1, \mathbf{k}_2) \Psi_k(\mathbf{k}_1) \Psi_i(\mathbf{k}_2) - \int_{\mathbf{k}_{123}=\mathbf{k}} \mathcal{K}_{kij}^{\text{FL}\Psi}(\mathbf{k}_1, \mathbf{k}_2, \mathbf{k}_3) \Psi_k(\mathbf{k}_1) \Psi_i(\mathbf{k}_2) \Psi_j(\mathbf{k}_3), \end{aligned} \quad (2.24)$$

valid up to cubic powers of Ψ , which is sufficient to construct LPT kernels up to third order, as we do in the following section. Notice that at very large scales both massive neutrinos and cb density perturbations are equal, $\alpha(k)$ becomes 1, and

$$A(k \rightarrow 0) \rightarrow A_0 = 4\pi G \bar{\rho}_m, \quad (2.25)$$

which simply means that neutrinos behave indistinguishably from CDM.

If $\alpha = 1$, the frame-lagging kernels vanish and we recover the standard equation for the longitudinal piece of the Lagrangian displacement in Λ CDM; see, e.g., [47]. Moreover, in that case eq. (2.24) becomes exact.

3 Perturbation Theory

In this section we find formal solutions to the Lagrangian displacements up to third order in PT. That is, as usual, we expand $\Psi = \Psi^{(1)} + \Psi^{(2)} + \Psi^{(3)} + \dots$, and solve eq. (2.24) in an iterative manner.

To linear order we use eq. (2.2) to connect density and Lagrangian displacement linear fields as

$$\Psi_i^{(1)}(\mathbf{k}, t) = i \frac{k_i}{k^2} \delta_{cb}^{(1)}(\mathbf{k}, t), \quad \text{with} \quad \delta_{cb}^{(1)}(\mathbf{k}, t) = \delta_{cb}^{(1)}(\mathbf{k}, t_0) D_+(\mathbf{k}, t), \quad (3.1)$$

and the scale-dependent linear growth function D_+ is the growing solution to

$$(\hat{\mathcal{T}} - A(k)) D_+(\mathbf{k}, t) = 0, \quad (3.2)$$

as obtained from eq. (2.24). At linear order, this yields $(\hat{\mathcal{T}} - A(k))[\Psi_{i,i}^{(1)}](\mathbf{k}) = 0$. To solve the above equation we start the evolution well inside the matter dominated Universe evolution phase, but once the neutrinos are non-relativistic, and use the fitting formula presented in [53] for the evolution of linear cb growth functions during the EdS epoch as initial conditions to eq. (3.2).

In general, the Lagrangian displacement to n -th order is

$$\Psi_i^{(n)}(\mathbf{k}, t) = \frac{i}{n!} \int_{\mathbf{k}_1 \dots \mathbf{k}_n = \mathbf{k}} L_i^{(n)}(\mathbf{k}_1, \dots, \mathbf{k}_n; t) D_+(\mathbf{k}_1, t) \dots D_+(\mathbf{k}_n, t) \delta_1 \dots \delta_n \quad (3.3)$$

where $\delta_1 = \delta_{cb}^{(1)}(\mathbf{k}_1, t_0)$, $\delta_2 = \delta_{cb}^{(1)}(\mathbf{k}_2, t_0)$, and so on. From eq. (3.1) we obtain

$$L_i^{(1)}(\mathbf{k}) = \frac{k_i}{k^2}. \quad (3.4)$$

Higher order solutions are found solving eq. (2.24) iteratively, as we do below.

3.1 2LPT

Now, we find the second order LPT kernel by inserting the linear solution (3.1) into the rhs of eq. (2.24). To do so, we first express the integrals containing the frame-lagging contributions in terms of linear density fields, which up to second order only appear through $\mathcal{K}_{ki}^{\text{FL}}$. We obtain

$$- \int_{\mathbf{k}_{12}=\mathbf{k}} \mathcal{K}_{ki}^{\text{FL}\Psi}(\mathbf{k}_1, \mathbf{k}_2) \Psi_k^{(1)}(\mathbf{k}_1) \Psi_i^{(1)}(\mathbf{k}_2) = - \frac{1}{2} \int_{\mathbf{k}_{12}=\mathbf{k}} K_{\text{FL}}^{(2)}(\mathbf{k}_1, \mathbf{k}_2) D_+(\mathbf{k}_1) D_+(\mathbf{k}_2) \delta_1 \delta_2 \quad (3.5)$$

with

$$K_{\text{FL}}^{(2)}(\mathbf{k}_1, \mathbf{k}_2) = (A(k) - A(k_1)) \frac{\mathbf{k}_1 \cdot \mathbf{k}_2}{k_2^2} + (A(k) - A(k_2)) \frac{\mathbf{k}_1 \cdot \mathbf{k}_2}{k_1^2}, \quad (3.6)$$

with $\mathbf{k} = \mathbf{k}_1 + \mathbf{k}_2$. Hence, to second order in PT, the equation of motion for the Lagrangian displacement is

$$(\hat{\mathcal{T}} - A(k))[\Psi_{i,i}^{(2)}](\mathbf{k}) = [\Psi_{i,j}^{(1)}\hat{\mathcal{T}}\Psi_{j,i}^{(1)}](\mathbf{k}) - \frac{A(k)}{2}[\Psi_{i,i}^{(1)}\Psi_{j,j}^{(1)} + \Psi_{i,j}^{(1)}\Psi_{j,i}^{(1)}](\mathbf{k}) - \frac{1}{2} \int_{\mathbf{k}_{12}=\mathbf{k}} K_{\text{FL}}^{(2)}(\mathbf{k}_1, \mathbf{k}_2) D_+(k_1) D_+(k_2) \delta_1 \delta_2. \quad (3.7)$$

The second order kernel becomes

$$L_i^{(2)}(\mathbf{k}_1, \mathbf{k}_2) = \frac{3}{7} \frac{k^i}{k^2} \left(\mathcal{A}(\mathbf{k}_1, \mathbf{k}_2) - \mathcal{B}(\mathbf{k}_1, \mathbf{k}_2) \frac{(\mathbf{k}_1 \cdot \mathbf{k}_2)^2}{k_1^2 k_2^2} \right). \quad (3.8)$$

\mathcal{A} and \mathcal{B} are scale and time dependent functions, defined as

$$\mathcal{A} = \frac{7}{3} \frac{D_{\mathcal{A}}(\mathbf{k}_1, \mathbf{k}_2)}{D_+(k_1) D_+(k_2)}, \quad \mathcal{B} = \frac{7}{3} \frac{D_{\mathcal{B}}(\mathbf{k}_1, \mathbf{k}_2)}{D_+(k_1) D_+(k_2)}, \quad (3.9)$$

with second order growth functions $D_{\mathcal{A},\mathcal{B}}$ the solutions to second order linear differential equations

$$(\hat{\mathcal{T}} - A(k)) D_{\mathcal{A}}(\mathbf{k}_1, \mathbf{k}_2) = \left[A(k) + K_{\text{FL}}^{(2)}(\mathbf{k}_1, \mathbf{k}_2) \right] D_+(k_1) D_+(k_2), \quad (3.10)$$

$$(\hat{\mathcal{T}} - A(k)) D_{\mathcal{B}}(\mathbf{k}_1, \mathbf{k}_2) = \left[A(k_1) + A(k_2) - A(k) \right] D_+(k_1) D_+(k_2), \quad (3.11)$$

with appropriate initial conditions to project out the homogeneous, linear order solution. For Λ CDM evolution with no massive neutrinos, $A(k) = \frac{3}{2} \Omega_m H^2$, hence $D_{\mathcal{A}} = D_{\mathcal{B}}$ are only time dependent,

$$D_{\mathcal{A}}^{f_{\nu}=0}(t) = \frac{3}{7} D_+^2(t) + \frac{4}{7} \left(\hat{\mathcal{T}} - \frac{3}{2} \Omega_m H^2 \right)^{-1} \left[\frac{3}{2} \Omega_m H^2 \left(1 - \frac{f^2}{\Omega_m} \right) \right], \quad (3.12)$$

with $f = d \log D_+(t) / d \log a(t)$ the logarithmic growth factor. For EdS, $\Omega_m = 1 = f$, and the second term in the rhs of the above equation vanishes, reducing the second order kernel [eq. (3.8)] to the well-known EdS result with $\mathcal{A} = \mathcal{B} = 1$.

It is useful to define the second order growth function $D^{(2)}$ as

$$k_i \Psi_i^{(2)} = \frac{i}{2} \int_{\mathbf{k}_{12}=\mathbf{k}} D^{(2)}(\mathbf{k}_1, \mathbf{k}_2) \delta_1 \delta_2. \quad (3.13)$$

At large scales $\mathcal{A} = \mathcal{B}$, as can be deduced by taking the limit $\mathbf{k} = 0$, $\mathbf{k}_1 = -\mathbf{k}_2 = \mathbf{p}$ in eqs. (3.10) and (3.11). Hence $D^{(2)}(-\mathbf{p}, \mathbf{p}) = 0$, as required since these wave-vector configurations correspond to planar collapse, for which Zeldovich approximation is exact [54]. We notice that this was possible because of cancellations provided by the frame-lagging terms, so these are particularly important to obtain a proper convergence at large scales. More generally, to leading order in k one gets

$$D^{(2)}(\mathbf{k} - \mathbf{p}, \mathbf{p}) = \frac{3}{7} \mathcal{C}_2 [D_+^{M_{\nu}=0}(t)]^2 \left(1 - (\hat{\mathbf{k}} \cdot \hat{\mathbf{p}})^2 \right) \frac{k^2}{p^2}, \quad (3.14)$$

for $k \ll p$, where \mathcal{C}_2 is a constant of order unity that depends very weakly on time. It also weakly depends on the wave-vector \mathbf{p} through $D_+(p, t)$, but it stabilizes beyond the

free-streaming scale since $D_+(p \gg k_{\text{FS}}, t) \approx [D_+^{M_\nu=0}(t)]^{1-3/5f_\nu}$ tends to a scale independent function [53]. Hence, more precisely, eq. (3.14) is valid for $k \ll k_{\text{FS}} \ll p$. For example, for massless neutrinos cosmologies $\mathcal{C}_2(z=0.5) \approx 1.005$, being slightly different to unity because of the contribution of the second term on the rhs of eq. (3.12); for degenerated massive neutrinos with total mass $M_\nu = 0.4$, we obtain $\mathcal{C}_2(z=0.5) \approx 0.93$.

3.2 Third order Lagrangian displacements

Now, in this subsection we find solutions to eq. (2.24) to third order in PT. We use the first and second order Lagrangian displacements to write the frame-lagging terms to third order as

$$\begin{aligned}
& -\frac{1}{6} \int_{\mathbf{k}_{12}=\mathbf{k}} K_{\text{FL}}^{(3)}(\mathbf{k}_1, \mathbf{k}_2, \mathbf{k}_3) D_+(k_1) D_+(k_2) D_+(k_3) \delta_1 \delta_2 \delta_3 \\
& \equiv - \int_{\mathbf{k}_{12}=\mathbf{k}} \mathcal{K}_{ki}^{\text{FL}\Psi}(\mathbf{k}_1, \mathbf{k}_2) (\Psi_k^{(2)}(\mathbf{k}_1) \Psi_i^{(1)}(\mathbf{k}_2) + \Psi_k^{(1)}(\mathbf{k}_1) \Psi_i^{(2)}(\mathbf{k}_2)) \\
& - \int_{\mathbf{k}_{123}=\mathbf{k}} \mathcal{K}_{kij}^{\text{FL}\Psi}(\mathbf{k}_1, \mathbf{k}_2, \mathbf{k}_3) \Psi_k^{(1)}(\mathbf{k}_1) \Psi_i^{(1)}(\mathbf{k}_2) \Psi_j^{(1)}(\mathbf{k}_3)
\end{aligned} \tag{3.15}$$

with

$$\begin{aligned}
K_{\text{FL}}^{(3)}(\mathbf{k}_1, \mathbf{k}_2, \mathbf{k}_3) &= 3(A(k) - A(k_1)) \left[\frac{\mathbf{k}_1 \cdot \mathbf{k}_{23}}{k_{23}^2} \frac{D^{(2)}(\mathbf{k}_2, \mathbf{k}_3)}{D_+(\mathbf{k}_2) D_+(\mathbf{k}_3)} - 2 \frac{(\mathbf{k}_1 \cdot \mathbf{k}_2)(\mathbf{k}_1 \cdot \mathbf{k}_3)}{k_2^2 k_3^2} \right] \\
&+ 3(A(k) - A(k_{23})) \frac{\mathbf{k}_1 \cdot \mathbf{k}_{23}}{k_1^2} \left[1 + 2 \frac{(\mathbf{k}_2 \cdot \mathbf{k}_3)}{k_3^2} + \frac{(\mathbf{k}_2 \cdot \mathbf{k}_3)^2}{k_2^2 k_3^2} + \frac{D^{(2)}(\mathbf{k}_2, \mathbf{k}_3)}{D_+(\mathbf{k}_2) D_+(\mathbf{k}_3)} \right],
\end{aligned} \tag{3.16}$$

and $\mathbf{k} = \mathbf{k}_1 + \mathbf{k}_2 + \mathbf{k}_3$. Now, the difference between the $\mathcal{K}_{ij\dots}^{\text{FL}\Psi}$ and K_{FL} kernels should be more clear, the former serve to expand $(\tilde{\alpha} - \alpha) \tilde{\delta}_{cb}$ on a Fourier series of non-linear Lagrangian displacements, while the latter serve to expand it on linear density fields.

To third order, the Lagrangian displacement equation of motion [eq. (2.24)] becomes

$$\begin{aligned}
(\hat{\mathcal{T}} - A(k))[\Psi_{i,i}^{(3)}](\mathbf{k}) &= [\Psi_{i,j}^{(2)} \hat{\mathcal{T}} \Psi_{j,i}^{(1)}](\mathbf{k}) + [\Psi_{i,j}^{(1)} \hat{\mathcal{T}} \Psi_{j,i}^{(2)}](\mathbf{k}) - A(k) [\Psi_{i,j}^{(2)} \Psi_{j,i}^{(1)} + \Psi_{i,i}^{(1)} \Psi_{j,j}^{(2)}](\mathbf{k}) \\
&- [\Psi_{i,k}^{(1)} \Psi_{k,j}^{(1)} \hat{\mathcal{T}} \Psi_{j,i}^{(1)}](\mathbf{k}) + \frac{A(k)}{3} [\Psi_{i,k}^{(1)} \Psi_{k,j}^{(1)} \Psi_{j,i}^{(1)}](\mathbf{k}) + \frac{A(k)}{6} [\Psi_{i,i}^{(1)} \Psi_{j,j}^{(1)} \Psi_{k,k}^{(1)}](\mathbf{k}) \\
&+ \frac{A(k)}{2} [\Psi_{i,l}^{(1)} \Psi_{l,j}^{(1)} \Psi_{j,i}^{(1)}](\mathbf{k}) - \frac{1}{6} \int_{\mathbf{k}_{12}=\mathbf{k}} K_{\text{FL}}^{(3)}(\mathbf{k}_1, \mathbf{k}_2, \mathbf{k}_3) D_+(\mathbf{k}_1) D_+(\mathbf{k}_2) D_+(\mathbf{k}_3) \delta_1 \delta_2 \delta_3.
\end{aligned} \tag{3.17}$$

Inserting the solutions for the first and second order Lagrangian displacements, a lengthy computation leads to⁷

$$\begin{aligned}
L_i^{(3)}(\mathbf{k}_1, \mathbf{k}_2, \mathbf{k}_3) &= \frac{k^i}{k^2} \left\{ \frac{5}{7} \left(\mathcal{A}^{(3)} - \mathcal{B}^{(3)} \frac{(\mathbf{k}_2 \cdot \mathbf{k}_3)^2}{k_2^2 k_3^2} \right) \left(1 - \frac{(\mathbf{k}_1 \cdot \mathbf{k}_{23})^2}{k_1^2 k_{23}^2} \right) \right. \\
&\quad \left. - \frac{1}{3} \left(\mathcal{C}^{(3)} - 3\mathcal{D}^{(3)} \frac{(\mathbf{k}_2 \cdot \mathbf{k}_3)^2}{k_2^2 k_3^2} + 2\mathcal{E}^{(3)} \frac{(\mathbf{k}_1 \cdot \mathbf{k}_2)(\mathbf{k}_2 \cdot \mathbf{k}_3)(\mathbf{k}_3 \cdot \mathbf{k}_1)}{k_1^2 k_2^2 k_3^2} \right) \right\},
\end{aligned} \tag{3.18}$$

⁷For details, we refer the reader to ref. [48], where an analogous computation is performed in the context of modified gravity.

plus a transverse piece that does not enter in 2-point, 1-loop statistics. The normalized growth functions are

$$\mathcal{A}^{(3)}, \mathcal{B}^{(3)}(\mathbf{k}_1, \mathbf{k}_2, \mathbf{k}_3) = \frac{7}{5} \frac{D_{\mathcal{A}, \mathcal{B}}^{(3)}(\mathbf{k}_1, \mathbf{k}_2, \mathbf{k}_3)}{D_+(k_1)D_+(k_2)D_+(k_3)}, \quad (3.19)$$

$$\mathcal{C}^{(3)}, \mathcal{D}^{(3)}, \mathcal{E}^{(3)}(\mathbf{k}_1, \mathbf{k}_2, \mathbf{k}_3) = \frac{D_{\mathcal{C}, \mathcal{D}, \mathcal{E}}^{(3)}(\mathbf{k}_1, \mathbf{k}_2, \mathbf{k}_3)}{D_+(k_1)D_+(k_2)D_+(k_3)}, \quad (3.20)$$

and third order growth functions

$$(\hat{\mathcal{T}} - A(k))D_{\mathcal{A}}^{(3)} = 3D_+(k_1)(A(k_1) + \hat{\mathcal{T}} - A(k))D_{\mathcal{A}}^{(2)}(\mathbf{k}_2, \mathbf{k}_3), \quad (3.21)$$

$$(\hat{\mathcal{T}} - A(k))D_{\mathcal{B}}^{(3)} = 3D_+(k_1)(A(k_1) + \hat{\mathcal{T}} - A(k))D_{\mathcal{B}}^{(2)}(\mathbf{k}_2, \mathbf{k}_3), \quad (3.22)$$

$$\begin{aligned} (\hat{\mathcal{T}} - A(k))D_{\mathcal{C}}^{(3)} &= 9D_+(k_1)(A(k_1) + \hat{\mathcal{T}} - 2A(k))D_{\mathcal{A}}^{(2)}(\mathbf{k}_2, \mathbf{k}_3) - 3A(k)D_+(k_1)D_+(k_2)D_+(k_3) \\ &\quad + 3K_{\text{FL}}^{(3)}(\mathbf{k}_1, \mathbf{k}_2, \mathbf{k}_3)D_+(k_1)D_+(k_2)D_+(k_3) \end{aligned} \quad (3.23)$$

$$(\hat{\mathcal{T}} - A(k))D_{\mathcal{D}}^{(3)} = 3D_+(k_1)(A(k_1) + \hat{\mathcal{T}} - 2A(k))D_{\mathcal{B}}^{(2)}(\mathbf{k}_2, \mathbf{k}_3) + 3A(k)D_+(k_1)D_+(k_2)D_+(k_3), \quad (3.24)$$

$$(\hat{\mathcal{T}} - A(k))D_{\mathcal{E}}^{(3)} = 3(3A(k_1) - A(k))D_+(k_1)D_+(k_2)D_+(k_3). \quad (3.25)$$

It is straightforward to check that for EdS evolution one has $\mathcal{A}^{(3)} = \mathcal{B}^{(3)} = \mathcal{C}^{(3)} = \mathcal{D}^{(3)} = \mathcal{E}^{(3)} = 1$.⁸ For Λ CDM with $f_{\nu} = 0$, these functions are only time dependent, at $z = 0$ $\mathcal{A}^{(3)} = \mathcal{B}^{(3)} \simeq 1.02$, $\mathcal{C}^{(3)} = \mathcal{D}^{(3)} = \mathcal{E}^{(3)} \simeq 1.01$ for typical cosmological parameter values.

We define $D^{(3)}(\mathbf{k}_1, \mathbf{k}_2, \mathbf{k}_3) = k_i L_i^{(3)}(\mathbf{k}_1, \mathbf{k}_2, \mathbf{k}_3)D_+(\mathbf{k}_1)D_+(\mathbf{k}_2)D_+(\mathbf{k}_3)$, hence

$$k_i \Psi_i^{(3)} = \frac{i}{6} \int_{\mathbf{k}_{12}=\mathbf{k}} D^{(3)}(\mathbf{k}_1, \mathbf{k}_2, \mathbf{k}_3) \delta_1 \delta_2 \delta_3. \quad (3.26)$$

The relevant configurations for computing 2-point statistics are double squeezed, for which $\mathbf{k}_1 = \mathbf{k}$ and $\mathbf{k}_3 = -\mathbf{k}_2 = \mathbf{p}$. Symmetrizing the third order kernel, and evaluating in this configuration we obtain

$$\begin{aligned} (\hat{\mathcal{T}} - A(k))D^{(3)s}(\mathbf{k}, -\mathbf{p}, \mathbf{p}) &= \left\{ D_+(p) \left(A(p) + \hat{\mathcal{T}} - A(k) \right) D^{(2)}(\mathbf{p}, \mathbf{k}) \left(1 - \frac{(\mathbf{p} \cdot (\mathbf{k} + \mathbf{p}))^2}{p^2 |\mathbf{p} + \mathbf{k}|^2} \right) \right. \\ &\quad + \left[(2A(k) - A(p) - A(|\mathbf{k} + \mathbf{p}|)) \left(\frac{D^{(2)}(\mathbf{p}, \mathbf{k})}{D_+(k)D_+(p)} + 1 + \frac{(\mathbf{k} \cdot \mathbf{p})^2}{k^2 p^2} \right) \right. \\ &\quad \left. \left. + A(k) - A(p) - K_{\text{FL}}^{(2)}(\mathbf{p}, \mathbf{k}) + K_{\text{FL}}^{(3)}(-\mathbf{p}, \mathbf{p}, \mathbf{k}) \right] D_+(k)D_+^2(p) \right\} \\ &+ (\mathbf{p} \rightarrow -\mathbf{p}), \end{aligned} \quad (3.27)$$

⁸Use the identities $\hat{\mathcal{T}}D_+^2 = 2D_+\hat{\mathcal{T}}D_+ + 2\dot{D}_+$ and $(\hat{\mathcal{T}} - \frac{3}{2}H^2)^{-1}[\frac{3}{2}H^2D_+^3] = \frac{1}{6}D_+^3$, where D_+ is the growing solution to $(\hat{\mathcal{T}} - \frac{3}{2}H^2)D_+ = 0$, and $H = 2/(3t)$.

with

$$\begin{aligned}
K_{\text{FL}}^{(3)}(-\mathbf{p}, \mathbf{p}, \mathbf{k}) &= (A(p) - A(k)) \frac{\mathbf{p} \cdot (\mathbf{k} + \mathbf{p})}{|\mathbf{k} + \mathbf{p}|^2} \frac{D^{(2)}(\mathbf{k}, \mathbf{p})}{D_+(k)D_+(p)} \\
&+ \frac{\mathbf{p} \cdot (\mathbf{k} + \mathbf{p})}{p^2} (A(|\mathbf{k} + \mathbf{p}|) - A(k)) \left[\frac{D^{(2)}(\mathbf{k}, \mathbf{p})}{D_+(k)D_+(p)} + 1 + \frac{(\mathbf{k} \cdot \mathbf{p})^2}{k^2 p^2} \right] \\
&+ \left[\frac{(k^2 + p^2)(\mathbf{k} \cdot \mathbf{p})^2}{k^2 p^4} + \frac{(k^2 + p^2)(\mathbf{k} \cdot \mathbf{p})}{k^3 p^3} \right] (A(|\mathbf{k} + \mathbf{p}|) - A(k)). \quad (3.28)
\end{aligned}$$

One can check that, due to cancellations provided by the frame-lagging terms, the symmetrized $D^{(3)s}(\mathbf{k} = 0, -\mathbf{p}, \mathbf{p}) \rightarrow 0$, or at leading order in k/p

$$D^{(3)s}(\mathbf{k}, -\mathbf{p}, \mathbf{p}) = \frac{7}{15} \mathcal{C}_3 [D_+^{M_\nu=0}(t)]^3 [1 - (\hat{\mathbf{k}} \cdot \hat{\mathbf{p}})^2]^2 \frac{k^2}{p^2}, \quad (3.29)$$

with \mathcal{C}_3 a constant of order unity. Hence, as in the case of the second order growth function, the leading term when $k \ll p$ is of order k^2/p^2 .

We end this section by noticing that in ref. [48] the LPT kernels for modified gravity theories were obtained using an approach that considers the evolution of a scalar field Klein-Gordon like equation. The kernels obtained in that work are a special case of the kernels obtained here.⁹ Hence, the method developed in this work is more general and find applications for scenarios that have additional scales than Λ CDM, such as modified gravity or dark matter clustering in the presence of massive neutrinos.

4 Neutrino density

In the presence of massive neutrinos, and at sufficiently late times such that relativistic components can be neglected, the Poisson equation becomes

$$\nabla_{\mathbf{x}}^2 \Phi(\mathbf{x}, t) = 4\pi G a^2 \bar{\rho}_m (f_{cb} \delta_{cb} + f_\nu \delta_\nu). \quad (4.1)$$

To our knowledge, a full, consistent analytic treatment of the non-linear nature of the neutrino density field does not exist in the literature. Various approximations have been tested in studies. In the pioneering work of [10] the δ_ν contribution is neglected to obtain the non-linear δ_{cb} , such that they use the EdS, SPT kernels, but using the linear power spectrum of the cb fluid, $P_{cb}^L(k)$, to compute the loop corrections. Other works approximate the neutrino overdensity by its linear value and use it as an external source to compute non-linear CDM overdensities [11, 12, 24]. In [17] it was noted that this approach violates momentum conservation yielding an incorrect behavior at large scales. In particular, SPT kernels do not follow $F_n \propto k^2$, and $(P_{\text{NL}} - P_{\text{L}})/P_{\text{L}} \propto k^2$, as $k \rightarrow 0$. The approach of [17], instead, evolves non-linear neutrino density fields by truncating the Boltzmann hierarchy at the Euler equation, and approximates the second moment of the phase-space distribution function (the velocity dispersion) to be proportional to an effective sound speed times the density contrast, as in

⁹One can check that for a function

$$A^{\text{MG}}(k) = \frac{3}{2} \Omega_m H^2 \left(1 + \frac{k^2/a^2}{3\Pi(k, a)} \right), \quad (3.30)$$

with $\Pi(k, a) = (k^2/a^2 + m_{\text{MG}}^2)/6\beta^2$, one recovers the kernels of [48].

[14, 19, 33] (see also Appendix C of [34]). Reference [21] performs non-linear perturbations around a Fermi-Dirac massive neutrino distribution to solve the coupled Boltzmann and CDM density field equations iteratively by expanding in powers of f_ν , keeping only the linear terms in f_ν .

In this work we will approximate

$$\tilde{\alpha}(k) \equiv \frac{\tilde{\delta}_\nu}{\tilde{\delta}_{cb}} \approx \frac{\tilde{\delta}_\nu^{(1)}}{\tilde{\delta}_{cb}^{(1)}}, \quad (4.2)$$

where we have returned to the Lagrangian treatment of the previous section — a tilde means the q -Fourier transform of Eulerian-coordinates valued function. Within this approximation, the non-linear neutrinos fluctuations become

$$\begin{aligned} \tilde{\delta}_\nu(\mathbf{k}) = \frac{\tilde{\delta}_\nu^{(1)}}{\tilde{\delta}_{cb}^{(1)}} \tilde{\delta}_{cb}(\mathbf{k}) &= \frac{\delta_\nu^{(1)}}{\delta_{cb}^{(1)}} \tilde{\delta}_{cb}(\mathbf{k}) + \frac{f_{cb}}{A_0 f_\nu} \int_{\mathbf{k}_{12}=\mathbf{k}} \mathcal{K}_{ki}^{\text{FL}\Psi}(\mathbf{k}_1, \mathbf{k}_2) \Psi_k(\mathbf{k}_1) \Psi_i(\mathbf{k}_2) \\ &+ \frac{f_{cb}}{A_0 f_\nu} \int_{\mathbf{k}_{12}=\mathbf{k}} \mathcal{K}_{kij}^{\text{FL}\Psi}(\mathbf{k}_1, \mathbf{k}_2, \mathbf{k}_3) \Psi_k(\mathbf{k}_1) \Psi_i(\mathbf{k}_2) \Psi_j(\mathbf{k}_3) + \dots \end{aligned} \quad (4.3)$$

where in the second equality we use eq. (2.19) and, by virtue of eq. (2.10), the neutrino density becomes written as a function of Lagrangian displacements and the ratio of linear overdensity fields. A similar approximation was adopted in [13, 15, 20] for Eulerian space, but notice that these are not exactly equal to ours, since “tilded” functions are given by eq. (2.8). Hence they carry the non-linear evolution provided by the Lagrangian displacements, as is manifest in the second equality of eq. (4.3), which contains corrections up to third order in PT. The authors of [17] argue that the approximation $\delta_\nu = (\delta_\nu^{(1)}/\delta_{cb}^{(1)})\delta_{cb}$ also violates momentum conservation. However, a good large scale behavior in our approach is provided by the frame-lagging terms, as was shown in [48] (sect. IV) in the context of MG, and we show in the following.

From the LPT kernels we construct the SPT kernels as [50, 55, 56]

$$F_2(\mathbf{k}_1, \mathbf{k}_2) = \frac{1}{2} (k_i L_i^{(2)}(\mathbf{k}_1, \mathbf{k}_2) + k_i k_j L_i^{(1)}(\mathbf{k}_1) L_j^{(1)}(\mathbf{k}_2)), \quad (4.4)$$

$$\begin{aligned} F_3^s(\mathbf{k}_1, \mathbf{k}_2, \mathbf{k}_3) &= \frac{1}{3} (k_i L_i^{(3)s}(\mathbf{k}_1, \mathbf{k}_2, \mathbf{k}_3) + k_i k_j (L_i^{(2)}(\mathbf{k}_1, \mathbf{k}_2) L_j^{(1)}(\mathbf{k}_3) + \text{cyclic}) \\ &+ k_i k_j k_k L_i^{(1)}(\mathbf{k}_1) L_j^{(1)}(\mathbf{k}_2) L_k^{(1)}(\mathbf{k}_3)). \end{aligned} \quad (4.5)$$

Using eq. (3.14) we obtain that $F_2(\mathbf{k}_1, \mathbf{k}_2) \propto k^2$ as $k = |\mathbf{k}_1 + \mathbf{k}_2| \rightarrow 0$ as required by momentum conservation. The case of the third order SPT kernel is challenging since the equations to construct $L_i^{(3)}$ are cumbersome for an analytical treatment, but using eq. (3.29) for the particular configuration used in constructing the 1-loop power spectrum it follows that $F_3^s(\mathbf{k}, -\mathbf{p}, \mathbf{p})$ goes as k^2 for $k \ll p$.

The SPT power spectrum is constructed as

$$P_{cb}^{\text{SPT}}(k) = P_{cb}^L(k) + P_{cb}^{22}(k) + P_{cb}^{13}(k), \quad (4.6)$$

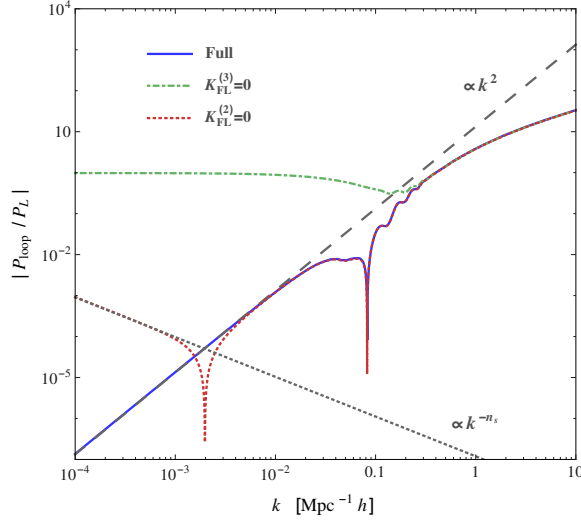


Figure 1. 1-loop correction to the matter power spectrum given by eqs. (4.4), (4.5) and (4.6) for massive neutrinos with total mass $M_\nu = 0.4 \text{ eV}$. We plot their ratio to the linear power spectrum showing that at large scales $(P^{\text{NL}} - P^L)/P^L \propto k^2$. The blue line shows the full power spectrum including the frame-lagging contributions. Dot-dashed green line shows the computation with no FL at third order, $K_{\text{FL}}^{(3)} = 0$, and the dotted red line shows the power spectrum without frame-lagging at second order, $K_{\text{FL}}^{(2)} = 0$.

with 1-loop contributions

$$P_{cb}^{22}(k) = 2 \int \frac{d^3p}{(2\pi)^3} [F_2(\mathbf{k} - \mathbf{p}, \mathbf{p})]^2 P_{cb}^L(|\mathbf{k} - \mathbf{p}|) P_{cb}^L(p), \quad (4.7)$$

$$P_{cb}^{13}(k) = 6 P_{cb}^L(k) \int \frac{d^3p}{(2\pi)^3} F_3^s(\mathbf{k}, -\mathbf{p}, \mathbf{p}) P_{cb}^L(p). \quad (4.8)$$

To see the importance of the frame-lagging contributions, and how they bring $P_{\text{loop}}/P_L \propto k^2$ at large scales, in figure 1 we show the ratio of the full SPT loop contributions power spectrum to the linear power spectrum, for massive neutrinos with $M_\nu = 0.4 \text{ eV}$, including the frame lagging terms (blue solid line), together with a power law $\propto k^2$ (dashed gray). The green dot-dashed line shows the computation by setting $K_{\text{FL}}^{(3)} = 0$, and the red dotted line the power spectrum without second order FL, $K_{\text{FL}}^{(2)} = 0$, but keeping the third order frame-lagging term; the two latter cases have UV divergences which manifest in a deviation of a k^2 behavior at large scales, while the full power spectrum does tend to $P_{\text{loop}} \propto k^2 P_L$ at very large scales. A similar plot is shown in ref. [17] (figure 8), to show that the approximation $\delta_\nu = \delta_\nu^{(1)}$ violates momentum conservation.

We take a closer look to the results of figure 1, when no frame-lagging are considered. By setting $K_{\text{FL}}^{(2)} = 0$, eq. (3.14) does not scale as k^2 but it tends to a constant value, which makes

$$P_{cb}^{\text{loop}}(k \rightarrow 0) \big|_{K_{\text{FL}}^{(2)}=0} \sim \frac{9}{98} \int_{p \gg k} \frac{dp}{4\pi^2} p^2 P_L^2(p) [\mathcal{A}(-\mathbf{p}, \mathbf{p})|_{\text{No FL}} - \mathcal{B}(-\mathbf{p}, \mathbf{p})]^2, \quad (4.9)$$

a constant — note that it is the frame-lagging term that makes $\mathcal{A} = \mathcal{B}$ for planar collapse. This explains the large scales behavior $P^{\text{loop}}/P^L \propto k^{-n_s}$, with n_s the primordial spectral index, for the red dotted curve in figure 1. Notice that this contribution comes entirely from P_{22} , more specifically from the term $k_i L_i^{(2)}$ in the F_2 function of eq. (4.4); on the other hand, with the frame-lagging, P_{22} scales as k^4 , as follows from eq. (3.14).

For $K_{\text{FL}}^{(3)} = 0$, the analysis is more challenging because the large-scale behavior becomes dominated by the third order LPT kernel. We numerically obtain that

$$P_{cb}^{\text{loop}}(k \rightarrow 0) \Big|_{K_{\text{FL}}^{(3)}=0} \propto P_L(k) \int_{p \gg k} \frac{dp}{4\pi^2} p^2 P_L(p), \quad (4.10)$$

which is expected for eq. (3.29) tending to a constant, instead of behaving as k^2/p^2 . The situation is worse than in the previous case, because here the result formally diverges for linear power spectra, $P_L(p) \propto p^n$ at high p , for $n \geq -3$. For the case of eq. (4.9), instead, the UV divergence appears for $n \geq -3/2$. The frame-lagging terms tame these UV divergences, rendering them to $n > 1/2$ and $n > -1$, for P_{22} and P_{13} respectively, which is a known result in SPT. Hence, without frame-lagging terms the theory poses UV divergences due to a failure of short-modes cancellations. Only when these are considered, the theory is well posed and large and small scales decouple.

One may be worried about the precise cancellations between $P_{22}(k)$ and $P_{13}(k)$ that occur at high- k . However, these are provided only by the terms containing linear displacement field kernels in eqs. (4.4) and (4.5), so they cancel in the same manner as in the Λ CDM. Technical difficulties, particularly for numerical integration, arise because P_{22} has IR divergences not only when the internal momentum is equal to zero, but also when its magnitude is equal to the external momentum; see, e.g. [57].

Now, coming back to eq. (4.3), we further take

$$\alpha(k) = \frac{\delta_\nu^{(1)}(k)}{\delta_{cb}^{(1)}(k)} \simeq \frac{T_\nu(k)}{T_{cb}(k)}, \quad (4.11)$$

where the equality holds true for adiabatic perturbations, being $T_\nu(k, z)$ and $T_{cb}(k, z)$ the transfer functions for neutrinos and the cb fluid, that relate the amplitude of linear density fields from their primordial initial state set by inflation up to redshift z . Hence, function $A(k)$, given by eq. (2.22), becomes

$$A(k, t) = 4\pi G \bar{\rho}_m \left(f_{cb} + f_\nu \frac{T_\nu(k, t)}{T_{cb}(k, t)} \right). \quad (4.12)$$

To compare our method with others approximations followed in the literature, we compute the growing function $D_+(k, t)$ from eq. (3.2) and use it to evolve a linear power spectrum obtained from the code **CAMB** [58] at $z = 10$ up to $z = 0$, and compare it with the output of **CAMB** at $z = 0$. In figure 2 we show the relative difference between these two quantities for different cases: a) the dashed red line is obtained by evolving the power spectrum of massive neutrinos, with $M_\nu = 0.4 \text{ eV}$, using $A(k, z) = 4\pi G \bar{\rho}_m$; b) blue dot-dashed uses $A(k) = A_0 = 4\pi G \bar{\rho}_m f_{cb}$; c) solid black uses $A(k, z)$ given by eq. (4.12); and, d) green dotted line evolves the massless neutrino case with $A(k, z) = 4\pi G \bar{\rho}_m$. We note that the for quasi-linear scales the approximation given by eq. (4.12) is very accurate. On the other hand,

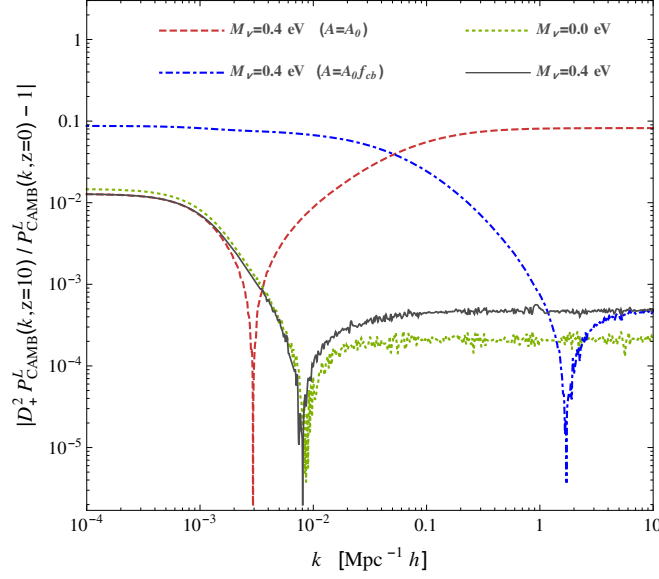


Figure 2. Relative differences of evolved auto power spectra of the cb fluid from redshift $z = 10$ to $z = 0$. The evolution is given by solving eq. (3.2), such that we compare $[D_+(k, z = 0)/D_+(k, z = 10)]^2 P_L(k, z = 10)$ with $P_L(k, z = 0)$, where both linear power spectra are obtained from CAMB. The dashed red line is obtained by evolving the power spectrum of massive neutrinos using $A(k, z) = 4\pi G\bar{\rho}_m = A_0$; blue dot-dashed uses $A(k, z) = 4\pi G\bar{\rho}_{cb} = A_0 f_{cb}$; solid black, $A(k, z)$ given by eq. (4.12); and green dotted line evolves the massless neutrino case.

the relative error of about 1% at very large scales is due to relativistic contributions to the Poisson equation, suppressed by factors (aH/k) . Such effect introduces an additional scale dependence which is not accounted for in eq. (3.2), but it does in Einstein-Boltzmann codes that compute the linear power spectrum. Notice that we will not use $D_+(k, t)$ to evolve linear fields, which are obtained directly from CAMB; however, both $A(k, t)$ and $D_+(k, t)$ are used to obtain the loop corrections to matter and tracer statistics.

We now test how good is the approximation $\delta_\nu = (T_\nu/T_{cb})\delta_{cb}$, and what is its range of validity. The m - m power spectrum can be decomposed as

$$P_{mm}(k) = f_{cb}^2 P_{cb}(k) + 2f_{cb}f_\nu P_{cb,\nu} + f_\nu^2 P_\nu(k), \quad (4.13)$$

where $P_{cb,\nu}$ is the cross-power spectrum of cb and neutrino fields, and P_ν the auto-power spectrum of neutrinos. Under our approximation for function $\alpha(k)$ given by eq. (4.11), the latter two are given by $P_{cb,\nu} = (T_\nu/T_{cb})P_{cb}$ and $P_\nu = (T_\nu/T_{cb})^2 P_{cb}$, which can be used to approximate P_{mm} as

$$P_{mm}^{\text{approx}}(k) = \left[f_{cb}^2 + 2f_\nu f_{cb} \left(\frac{T_\nu(k)}{T_{cb}(k)} \right) + f_\nu^2 \left(\frac{T_\nu(k)}{T_{cb}(k)} \right)^2 \right] P_{cb}(k). \quad (4.14)$$

In the left panel of figure 3 we plot the ratio of nonlinear power spectrum cb to the nonlinear power spectrum of the total matter field ($cb + \nu$), both obtained directly from the QUIJOTE suite of simulations (below, in the following section, we briefly describe the specifications of these simulations). We are doing this for cosmologies with massive neutrinos

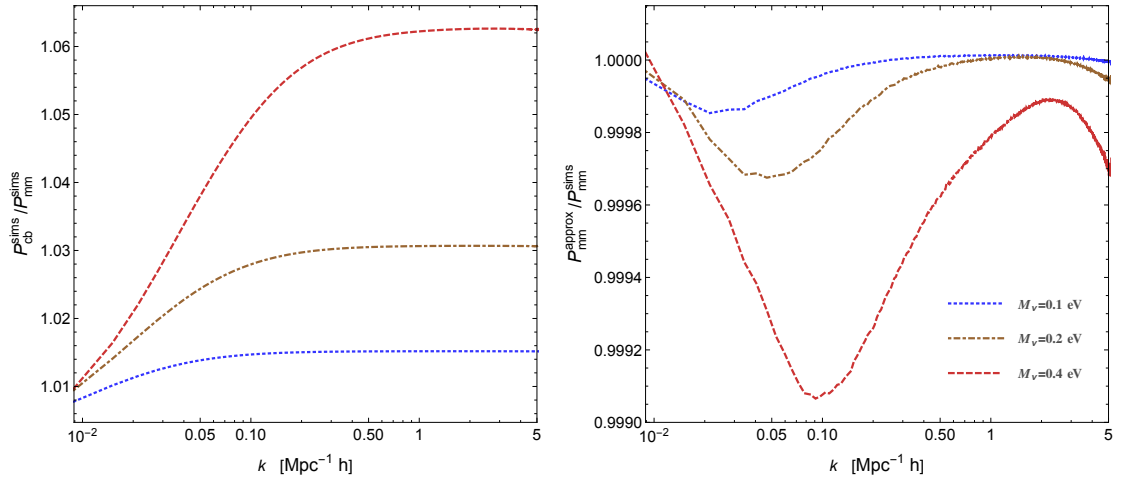


Figure 3. Comparison of non-linear power spectra for the different cases considered in this work: $M_\nu = 0.1, 0.2, 0.4$ eV at redshift $z = 0.5$; shown in dotted blue, dot-dashed brown and dashed red lines. The left panel show the ratios of the cb - cb power spectrum to the m - m power spectrum, both obtained from the simulations. The right panel shows the ratio of the approximated m - m power spectrum, given by eq. (4.14), to the m - m power spectrum obtained from the simulations. The difference between the latter is smaller than the 0.1% for all models considered here up to $k = 5 \text{ Mpc}^{-1} h$, showing that the approximation $\delta_\nu = (T_\nu/T_{cb})\delta_{cb}$ works also at highly non-linear scales.

$M_\nu = 0.1, 0.2, 0.4$ eV corresponding to $f_{cb} = 0.9925, 0.985, 0.97$, and consider redshift $z = 0.5$. At very large scales the matter power spectrum, P_{mm}^{sims} , for the three models tend to P_{cb}^{sims} because neutrino and cb overdensities behave equally. On the other hand, at small scales neutrinos do not cluster, and P_{mm}^{sims} become suppressed by factors f_{cb}^2 , tending to $f_{cb}^2 P_{cb}^{\text{sims}}$, so the ratios go to the constants $1/f_{cb}^2$.

In the right panel of figure 3 we plot the ratios of the approximation given in eq. (4.14), with $P_{cb} = P_{cb}^{\text{sims}}$ obtained from the simulations, to the matter power spectrum P_{mm}^{sims} . These two power spectra differ by less than 0.1% over the interval $k \in (0.009, 5) \text{ Mpc}^{-1} h$ for all considered models. This analysis shows that the approximation given by eq. (4.11) is valid well inside the non-linear regime.

5 Real space correlation function

In this section, we construct the real space correlation function for tracers within the CLPT framework, using the LPT for CDM in the presence of massive neutrinos developed in the previous sections. Here, we will compare our analytical results only to simulated particles, both cb and total matter. A comparison to CDM halos is performed in section 7.

We will assume the existence of a Lagrangian biasing function F that relates the density fluctuations of tracers $\delta_X(\mathbf{q})$ with a set of operators constructed out of the CDM Lagrangian overdensities. Our biasing scheme is simple since we introduce only local and curvature biases, which shows to provide the level of accuracy necessary to match the simulations we consider. If desired, tidal bias can be introduced along the lines of ref. [41], with small modifications due to the generalized kernels used [39]. Hence, cb and tracer initial densities

are related by

$$1 + \delta_X(\mathbf{q}) = F(\delta_{cb}, \nabla^2 \delta_{cb}) = \int \frac{d^2 \mathbf{\Lambda}}{(2\pi)^2} \tilde{F}(\mathbf{\Lambda}) e^{i\mathbf{D} \cdot \mathbf{\Lambda}}. \quad (5.1)$$

In the second equality $\tilde{F}(\mathbf{\Lambda})$ is the Fourier transform of $F(\mathbf{D})$, with arguments $\mathbf{D} = (\delta_{cb}, \nabla^2 \delta_{cb})$ and spectral parameters $\mathbf{\Lambda} = (\lambda, \eta)$, dual to \mathbf{D} . Assuming number conservation of tracers, $[1 + \delta_X(\mathbf{x})] d^3 x = [1 + \delta_X(\mathbf{q})] d^3 q$, one obtains

$$1 + \delta_X(\mathbf{x}) = \int \frac{d^3 k}{(2\pi)^3} \int d^3 q e^{i\mathbf{k} \cdot (\mathbf{x} - \mathbf{q})} \int \tilde{F}(\mathbf{\Lambda}) e^{i\mathbf{D} \cdot \mathbf{\Lambda} - i\mathbf{k} \cdot \mathbf{\Psi}}, \quad (5.2)$$

which evolves initially biased tracer densities using the map of eq. (2.1) between Lagrangian and Eulerian coordinates. Renormalized bias parameters are obtained through [59, 60]

$$b_{nm} = \int \frac{d\mathbf{\Lambda}}{(2\pi)^2} \tilde{F}(\mathbf{\Lambda}) e^{-\frac{1}{2} \mathbf{\Lambda}^T \Sigma \mathbf{\Lambda}} (i\lambda)^n (i\eta)^m, \quad (5.3)$$

with covariance matrix components $\Sigma_{11} = \langle \delta_{cb}^2 \rangle$, $\Sigma_{12} = \Sigma_{21} = \langle \delta_{cb} \nabla^2 \delta_{cb} \rangle$ and $\Sigma_{22} = \langle (\nabla^2 \delta_{cb})^2 \rangle$. We identify $b_n = b_{n0}$ with the local bias parameter of order n , and $b_{\nabla^2 \delta} = b_{01}$ with the curvature bias parameter. The correlation function $\xi_X(r)$ for tracer X is obtained from eqs. (5.1), (5.2) and (5.3) by using the standard methods of CLPT [36, 60–63],

$$\begin{aligned} 1 + \xi_{X,cb}(r) = & \int \frac{d^3 q}{(2\pi)^{3/2} |\mathbf{\Lambda}_L|^{1/2}} e^{-\frac{1}{2} (\mathbf{r} - \mathbf{q})^T \mathbf{\Lambda}_L^{-1} (\mathbf{r} - \mathbf{q})} \left\{ 1 - \frac{1}{2} A_{ij}^{loop} G_{ij} + \frac{1}{6} \Gamma_{ijk} W_{ijk} \right. \\ & + b_1 (-2U_i g_i - A_{ij}^{10} G_{ij}) + b_1^2 (\xi_L - U_i U_j G_{ij} - U_i^{11} g_i) + b_2 \left(\frac{1}{2} \xi_L^2 - U_i^{20} g_i - U_i U_j G_{ij} \right) \\ & \left. - 2b_1 b_2 \xi_L U_i g_i + 2(1 + b_1) b_{\nabla^2 \delta} \nabla^2 \xi_L + b_{\nabla^2 \delta}^2 \nabla^4 \xi_L \right\}, \end{aligned} \quad (5.4)$$

where we are using the label “ cb ” in $\xi_{X,cb}$ to distinguish that we are biasing the cb fluid and not the whole matter density $\delta_m = f_{cb} \delta_{cb} + f_\nu \delta_\nu$. The matrix $A_{ij}^L(\mathbf{q}) = \langle \Delta_i^{(1)} \Delta_j^{(1)} \rangle_c$, with $\Delta_i = \Psi_i(\mathbf{q}_2) - \Psi_i(\mathbf{q}_1)$, is the correlation of the difference of linear displacement fields for initial positions separated by a distance $\mathbf{q} = \mathbf{q}_2 - \mathbf{q}_1$,

$$A_{ij}^L(\mathbf{q}) = 2 \int \frac{d^3 p}{(2\pi)^3} (1 - e^{i\mathbf{p} \cdot \mathbf{q}}) \frac{p_i p_j}{p^4} P_{cb}^L(p), \quad (5.5)$$

and the tensors $g_i = (\mathbf{\Lambda}_L^{-1})_{ij} (r_j - q_j)$, $G_{ij} = (\mathbf{\Lambda}_L^{-1})_{ij} - g_i g_j$, and $\Gamma_{ijk} = (\mathbf{\Lambda}_L^{-1})_{\{ij} g_{k\}} - g_i g_j g_k$. We further use the linear correlation function

$$\xi_L(q) = \int \frac{d^3 p}{(2\pi)^3} e^{i\mathbf{p} \cdot \mathbf{q}} P_{cb}^L(p), \quad (5.6)$$

and the functions

$$W_{ijk} = \langle \Delta_i \Delta_j \Delta_k \rangle_c, \quad A_{ij}^{mn} = \langle \delta_{cb}^m(\mathbf{q}) \delta_{cb}^n(0) \Delta_i \Delta_j \rangle_c, \quad U_i^{mn} = \langle \delta_{cb}^m(\mathbf{q}) \delta_{cb}^n(0) \Delta_i \rangle_c, \quad (5.7)$$

such that $A_{ij}^{loop} \equiv A_{ij}^{00} - A_{ij}^L$, and $U_i \equiv U_i^{00}$. For example, the linear piece of function U_i is

$$U_i^L(\mathbf{q}) = -i \int \frac{d^3 p}{(2\pi)^3} e^{i\mathbf{p} \cdot \mathbf{q}} \frac{p^i}{p^2} P_{cb}^L(p). \quad (5.8)$$

The CLPT correlation function given by eq. (5.4) has the same structure that in the massless neutrino Λ CDM model. The differences with the $f_\nu = 0$ case appear through the functions U_i , A_{ij} , W_{ijk} , since they are ultimately constructed out of the LPT kernels. In Appendix A we show how these reduce to integrals of the kernels and linear power spectra.

The correlation function for tracers can be obtained as well by considering the bias of the auto-correlation function with respect to the total matter field, $\xi_{X,m}(r)$, that we approximate by replacing P_{cb}^L by $P_m^L = f_{cb}^2 P_{cb}^L + 2f_{cb}f_\nu P_{cb,\nu}^L + f_\nu^2 P_\nu^L$ in the linear functions appearing in eq. (5.4) (A_{ij}^L , U_i^L and ξ_L) and multiplying by f_{cb}^2 all loop contributions.¹⁰ Our approach is analogous to the usually followed for the SPT power spectrum, that approximates $P_m^{\text{SPT}} = f_{cb}^2 P_{cb}^{\text{SPT}} + 2f_{cb}f_\nu P_{cb,\nu}^{\text{SPT}} + f_\nu^2 P_\nu^{\text{SPT}}$. By doing so, we neglect the loop contributions in the correlation function coming from non-linear terms of δ_ν . Although our method is in apparent inconsistency with the general treatment given in the previous sections, these loops contributions are smaller than those coming from CDM densities and further suppressed by factors f_ν , hence the error we are committing is very small as long as the neutrino masses are not very large.

We want to assess the goodness of our analytical model by comparing directly to the particles of N -body simulations. Later, in section 7, we will compare to tracers. To this end, we use measurements from the QUIJOTE N -body simulation suite [40]. The fiducial cosmology in the QUIJOTE suite has $\Omega_m = 0.3175$, $\Omega_b = 0.049$, $h = 0.6711$, $n_s = 0.9624$, and $\sigma_8 = 0.834$, and $M_\nu = 0$ eV. There are also three massive neutrino cosmologies (assuming three degenerate massive neutrinos) with total mass $M_\nu = 0.1, 0.2, 0.4$ eV corresponding to $f_\nu = 0.0075, 0.015, 0.03$, respectively. The simulations volume is $(1 \text{ Gpc } h^{-1})^3$, and uses 512^3 CDM particles for the massless neutrino cosmology, and 512^3 CDM and 512^3 neutrino particles for the massive neutrino cosmologies. Note that in these simulations σ_8 is kept fixed, such that the primordial amplitude A_s is different for each model. To reduce the sample variance in the simulation measurements, we use 100 realizations at each cosmology.

By comparing to the simulated particles we get a direct test of our theory since in this case we have no free parameters. To this end we set all bias parameters to zero and perform the integral in eq. (5.4). We show the analytical results together with the simulated data in figure 4 for the CDM particles (cb - cb) in the top panels, and to all particles (m - m), including also the massive neutrinos, in the bottom panels. The differences among the models are dominated by their large scale, primordial amplitudes; hence, to isolate the effects of late time clustering, we have multiplied the particle real space correlation functions by constants equal to “factor” = $P_L^{M_\nu=0.4}(k_0)/P_L^{M_\nu=0,0.1,0.2,0.4}(k_0) = 1.29, 1.22, 1.14, 1$, with $k_0 = 10^{-4} \text{ Mpc}^{-1}h$, such that the corresponding power spectrum in all models have approximately the same primordial amplitude $A_s = 2.74 \times 10^{-9}$. The figures on the right column show the ratios $\xi/\xi^{M_\nu=0}$ (including the constant factors) of the different massive cases to the massless neutrino correlation function, with the shaded region showing the RMS error of the simulated data. We find that our analytical approach show the same level of accuracy for all models, being consistent with the data down to $r = 20 \text{ Mpc } h^{-1}$, being this the standard level of precision provided by CLPT [36, 61]. Below this scale the predictions of CLPT overshoot the N -body simulated data.

¹⁰An alternative is to use $\xi_{X,m}(r) = f_{cb}^2 \xi_{X,cb}^{\text{CLPT}}(r) + (1+b_1)^2 (2f_{cb}f_\nu \xi_{cb,\nu}^{\text{ZA}}(r) + f_\nu^2 \xi_\nu^{\text{ZA}}(r))$, where the Zeldovich approximation-like correlation functions $\xi_{cb,\nu}^{\text{ZA}}(r)$ and $\xi_\nu^{\text{ZA}}(r)$ are obtained by taking only the “1” term inside the brackets of eq. (5.4) and substituting P_{cb} by $P_{cb,\nu}$ and P_ν , respectively, in eq. (5.5). Both approaches yield similar results, with differences smaller than the 1% at all scales.

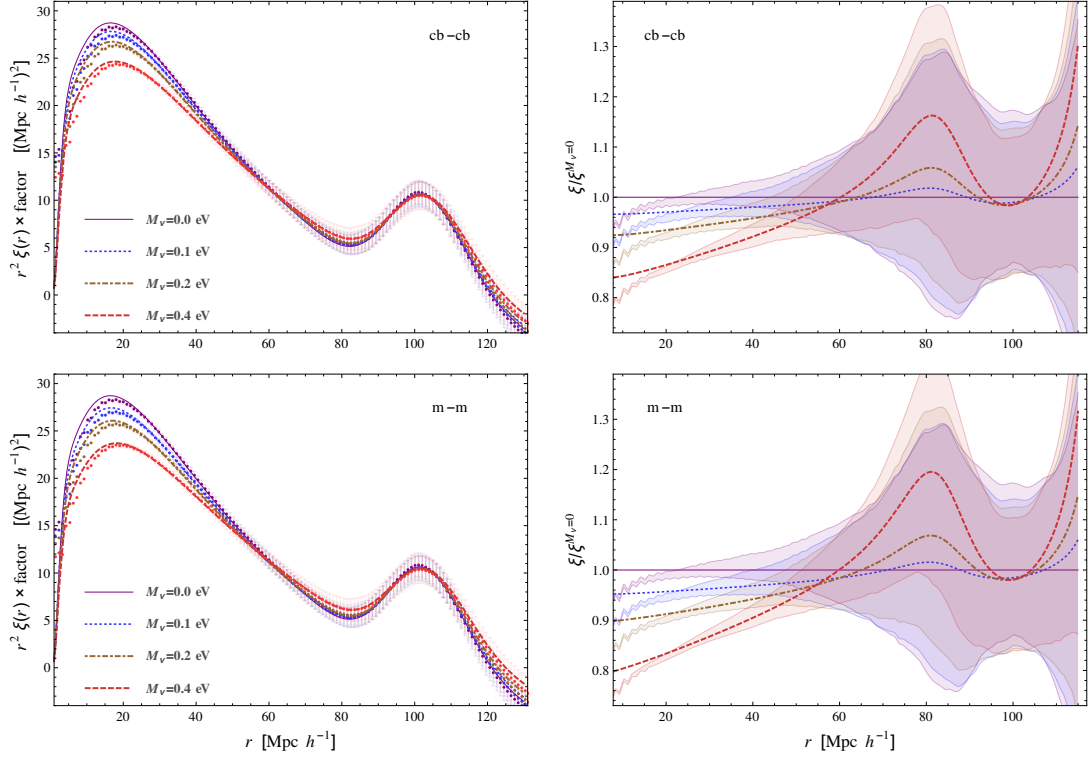


Figure 4. Particles real space correlation function at $z = 0.5$ for $M_\nu = 0.0$ eV (solid purple line), $M_\nu = 0.1$ eV (dotted blue), $M_\nu = 0.2$ eV (dot-dashed brown) and $M_\nu = 0.4$ eV (dashed red) compared to N -body simulations data (dots). The upper figures show the cb fluid auto-correlation functions and the lower figures the $m = cb + \nu$ auto-correlation functions. For visualization purposes, we have multiplied the results by constant factors $P_L^{M_\nu=0.4}(k_0)/P_L^{M_\nu=0,0.1,0.2,0.4}(k_0)$, with $k_0 = 10^{-4}$, such that at large scales the corresponding power spectrum in all models have approximately the same amplitude. The right panels show the ratios over the massless neutrino case, with the shaded regions the simulated data RMS errors.

6 Redshift-space correlation function

In this section we turn our attention to the effects of RSD in the 2-point statistics. As before, we will present the whole theory for biased tracers and we will compare the analytical results only to simulated particles. In section 7, we will compare to CDM halos.

An object located at a comoving real space position \mathbf{x} is observed to be at an apparent, redshift-space position \mathbf{s} , due to the Doppler effect induced by its peculiar velocity, $a\dot{\Psi}$, relative to the Hubble flow. Hence, both coordinate systems are related by $\mathbf{s} = \mathbf{x} + \mathbf{u}$, with “velocity” \mathbf{u} defined as

$$\mathbf{u} \equiv \hat{\mathbf{n}} \frac{\dot{\Psi} \cdot \hat{\mathbf{n}}}{H}, \quad (6.1)$$

where we adopted the plane-parallel approximation, for which $\hat{\mathbf{n}}$ is a constant vector in the direction of the survey, instead of being equal to the position unit vector $\hat{\mathbf{x}}$. The map between Lagrangian coordinates and redshift space Eulerian positions becomes

$$\mathbf{s} = \mathbf{q} + \Psi + \hat{\mathbf{n}} \frac{\dot{\Psi} \cdot \hat{\mathbf{n}}}{H}. \quad (6.2)$$

Conservation of number of objects, $[1 + \delta_s(\mathbf{s})]d^3s = [1 + \delta(\mathbf{x})]d^3x$, yields

$$(2\pi)^3\delta_D(\mathbf{k}) + \delta_s(\mathbf{k}) = \int d^3x [1 + \delta(\mathbf{x})] e^{i\mathbf{k}\cdot(\mathbf{x}+\mathbf{u}(\mathbf{x}))}, \quad (6.3)$$

and the redshift-space correlation function becomes [64]

$$1 + \xi_s(\mathbf{s}) = \int \frac{d^3k}{(2\pi)^3} d^3x e^{i\mathbf{k}\cdot(\mathbf{s}-\mathbf{x})} [1 + \mathcal{M}(\mathbf{k}, \mathbf{x})], \quad (6.4)$$

with pairwise velocity generating function

$$1 + \mathcal{M}(\mathbf{k}, \mathbf{x}) = \left\langle (1 + \delta_1)(1 + \delta_2) e^{i\mathbf{k}\cdot\Delta\mathbf{u}} \right\rangle, \quad (6.5)$$

where $\Delta\mathbf{u} = \mathbf{u}(\mathbf{x}_2) - \mathbf{u}(\mathbf{x}_1)$, $\mathbf{x} = \mathbf{x}_2 - \mathbf{x}_1$ and $\delta_1 = \delta_{cb}(\mathbf{x}_1)$, $\delta_2 = \delta_{cb}(\mathbf{x}_2)$. We expand the pairwise velocity generating function in cumulants as [63, 64]

$$1 + \mathcal{M}(\mathbf{k}, \mathbf{x}) = [1 + \xi(x)] \exp \left[ik_i v_{12,i}(\mathbf{x}) - \frac{1}{2} k_i k_j \sigma_{12,ij}^2(\mathbf{x}) + \dots \right], \quad (6.6)$$

with $\xi(x)$ the real space correlation function, \mathbf{v}_{12} the pairwise velocity and σ_{12}^2 the pairwise velocity dispersion, with components

$$v_{12,i}(\mathbf{x}) = \frac{\langle (1 + \delta_1)(1 + \delta_2) \Delta u_i \rangle_c}{1 + \xi(x)}, \quad (6.7)$$

$$\sigma_{12,ij}^2(\mathbf{x}) = \frac{\langle (1 + \delta_1)(1 + \delta_2) \Delta u_i \Delta u_j \rangle_c}{1 + \xi(x)} - v_{12,i}(\mathbf{x}) v_{12,j}(\mathbf{x}). \quad (6.8)$$

To be consistent in including all 1-loop contributions, one should also consider the third and fourth cumulant of the pairwise velocity generating function. However, by keeping only up to the second cumulant, as in eq. (6.6), the \mathbf{k} -integral in eq. (6.4) can be performed analytically. By doing so, one obtains [63]

$$1 + \xi_s(\mathbf{s}) = \int \frac{d^3x}{(2\pi)^{3/2} |\sigma_{12}^2|^{1/2}} [1 + \xi(x)] \exp \left[-\frac{1}{2} (\mathbf{s} - \mathbf{x} - \mathbf{v}_{12}) [\sigma_{12}^2]^{-1} (\mathbf{s} - \mathbf{x} - \mathbf{v}_{12}) \right], \quad (6.9)$$

which is the GSM expression for the redshift-space correlation function [37, 64, 65].

The method to obtain expressions for the velocity and velocity dispersion is very similar as in the Λ CDM case. However one should consider that in the presence of massive neutrinos, the growth function D_+ is scale dependent, and hence the logarithmic growth factor

$$f(k, t) = \frac{d \ln D_+(k, t)}{d \ln a(t)}, \quad (6.10)$$

also becomes scale dependent. For notational convenience, we define $f_0 \equiv f(k_0, t)$, with k_0 an arbitrary scale that we choose to correspond to a sufficiently long mode, such that $f_0 = f^{M_\nu=0}$. With this, the time derivative of the Lagrangian displacement at perturbative order n can be written as

$$\dot{\Psi}_i^{(n)}(\mathbf{q}) = n f_0 H \int_{\mathbf{k}_1 \dots \mathbf{k}_n = \mathbf{k}} \frac{i}{n!} L_i^{f(n)}(\mathbf{k}_1, \dots, \mathbf{k}_n; t) \delta(\mathbf{k}_1) \dots \delta(\mathbf{k}_n), \quad (6.11)$$

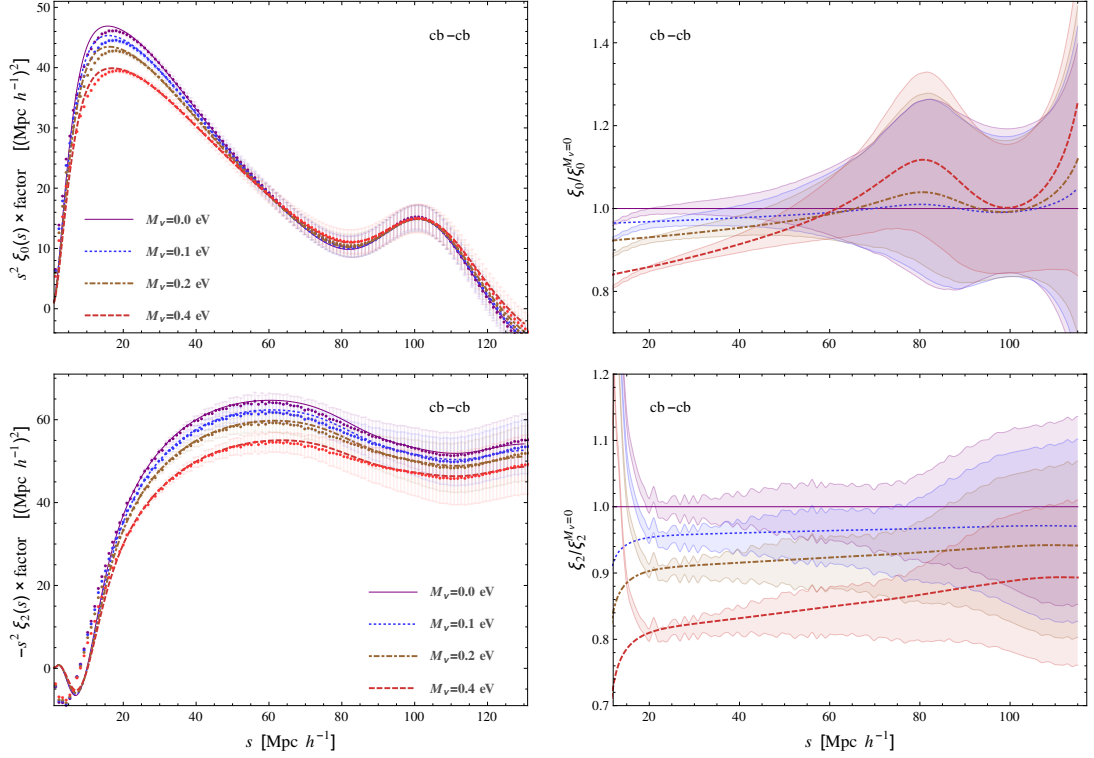


Figure 5. *cb* particles redshift space correlation functions at $z = 0.5$. The upper figures show the monopole and the lower figures the quadrupole. The right panels show the ratios over the massless case, with the shaded regions the simulated data RMS errors. We use an EFT parameter $\alpha_\sigma = 13.5/f_0^2 \times (\text{Mpc } h^{-1})^2$ in all cases.

with kernels

$$L_i^{f(n)}(\mathbf{k}_1, \dots, \mathbf{k}_n) = \frac{f(k_1) + \dots + f(k_n)}{nf_0} L_i(\mathbf{k}_1, \dots, \mathbf{k}_n) + \frac{1}{nf_0 H} \dot{L}_i^{(n)}(\mathbf{k}_1, \dots, \mathbf{k}_n). \quad (6.12)$$

If f is scale independent, and we further use the static kernels approximation, we obtain the standard result $\dot{\Psi}^{(n)} = nfH\Psi^{(n)}$, widely used for Λ CDM and exact for EdS kernels. We employ CLPT to obtain the pairwise velocity and velocity dispersion for the *cb* fluid, see [38, 41],

$$\begin{aligned} [1 + \xi_{X,cb}(r)] v_{12,i}(\mathbf{r}) = f_0 \int \frac{d^3q e^{-\frac{1}{2}(\mathbf{r}-\mathbf{q})^T \mathbf{A}_L^{-1}(\mathbf{r}-\mathbf{q})}}{(2\pi)^{3/2} |\mathbf{A}_L|^{1/2}} & \left\{ -g_r \dot{A}_{ri} - \frac{1}{2} G_{rs} \dot{W}_{rsi} \right. \\ & + b_1 \left(2\dot{U}_i - 2g_r \dot{A}_{ri}^{10} - 2G_{rs} U_r \dot{A}_{si} \right) + b_1^2 \left(\dot{U}_i^{11} - 2g_r U_r \dot{U}_i - g_r \dot{A}_{ri} \xi_L \right) \\ & \left. + b_2 \left(\dot{U}_i^{20} - 2g_r U_r \dot{U}_i \right) + 2b_1 b_2 \xi_L \dot{U}_i + 2b_{\nabla^2 \delta} \nabla_i \xi_L \right\}, \end{aligned} \quad (6.13)$$

and

$$\begin{aligned}
[1 + \xi_{X,cb}(r)]\sigma_{12,ij}^2(\mathbf{r}) = f_0^2 \int \frac{d^3q e^{-\frac{1}{2}(\mathbf{r}-\mathbf{q})^T \mathbf{A}_L^{-1}(\mathbf{r}-\mathbf{q})}}{(2\pi)^{3/2} |\mathbf{A}_L|^{1/2}} & \left\{ \ddot{A}_{ij} - g_r \ddot{W}_{rij} - G_{rs} \dot{A}_{ri} \dot{A}_{sj} \right. \\
& \left. + \alpha_\sigma \delta_{ij} + 2b_1 \left(\ddot{A}_{ij}^{10} - g_r \dot{A}_{r\{i} \dot{U}_{j\}} - g_r U_r \ddot{A}_{ij} \right) + b_1^2 \left(\xi_L \ddot{A}_{ij} + 2\dot{U}_i \dot{U}_j \right) + 2b_2 \dot{U}_i \dot{U}_j \right\}, \quad (6.14)
\end{aligned}$$

with $\xi_{X,cb}(r)$ the CLPT tracers correlation function in eq. (5.4), and

$$\begin{aligned}
\dot{A}_{ij}^{mn}(\mathbf{q}) &= \frac{1}{f_0 H} \langle \delta_1^m \delta_2^n \Delta_i \dot{\Delta}_j \rangle, & \ddot{A}_{ij}^{mn}(\mathbf{q}) &= \frac{1}{f_0^2 H^2} \langle \delta_1^m \delta_2^n \ddot{\Delta}_i \dot{\Delta}_j \rangle, \\
\dot{W}_{ijk} &= \frac{1}{f_0 H} \langle \Delta_i \Delta_j \dot{\Delta}_k \rangle, & \ddot{W}_{ijk} &= \frac{1}{f_0^2 H^2} \langle \Delta_i \dot{\Delta}_j \dot{\Delta}_k \rangle, \\
\dot{U}^{mn}(\mathbf{q}) &= \frac{1}{f_0 H} \langle \delta_1^m \delta_2^n \dot{\Delta}_i \rangle, \quad (6.15)
\end{aligned}$$

and, as before, we omitted to write the superscripts m, n when these are zero; e.g. $\dot{A}_{ij} \equiv \dot{A}_{ij}^{00}$. The scale dependence of $f(k)$ is included in the above “dotted” functions, and we have factorized the factors f_0 to keep the same notation, standard in the literature, as for the massless neutrinos case. In Appendix A we show how these “dotted” A , U and W functions are computed numerically.

Following [41], we have included an Effective Field Theory (EFT) counterterm $\alpha_\sigma \delta_{ij}$ to $\ddot{A}_{ij} + 2b_1 \ddot{A}_{ij}^{10}$, since this combination of functions approach to a non-vanishing, bias-dependent constant at large separation q (times the Kronecker δ_{ij}), that is very sensitive to small scale physics, mainly to the zero-lag correlator $\langle \dot{\Psi}_i(0) \dot{\Psi}_j(0) \rangle$ which cannot be treated perturbatively. The EFT parameter α_σ contributes to the pairwise velocity dispersion tensor as

$$\alpha_\sigma f_0^2 \frac{1 + \xi_{cb}^{\text{ZA}}(r)}{1 + \xi_{X,cb}^{\text{CLPT}}(r)} \delta_{ij} \in \sigma_{12,ij}^2(\mathbf{r}), \quad (6.16)$$

hence it accommodates well on early works that noticed the necessity of adding a constant shift to match the large scales pairwise velocity dispersion observed in N -body simulations [37, 38]. There are several others EFT counterterms entering the CLPT correlation function and the pairwise velocity and velocity dispersion, but they are either degenerated with curvature bias or subdominant with respect to the contribution of eq. (6.16) (see the discussion in [41]), so in this work we keep only α_σ . Since this EFT parameter modifies the second cumulant of the pairwise velocity generation function, its effect on the redshift space monopole correlation function is small, while the quadrupole is quite sensitive to it, particularly at intermediate scales $r < 40 \text{ Mpc } h^{-1}$.

The cb auto correlation function is obtained by substituting eqs. (5.4), (6.13) and (6.14) into eq. (6.9). In figure 5 we show the monopole (top panels) and quadrupole (bottom panels) of the correlation function for the unbiased case, though we keep the EFT parameter since it is necessary to match the quadrupole simulated data. We have multiplied each correlation function by the same factors as in figure 4. The right panels show the ratios to the massless neutrino case with the shaded regions the RMS errors. We have used an EFT parameter $\alpha_\sigma = 13.5/f_0^2 \times \text{Mpc}^2 h^{-2}$, with $f_0 = 0.76$ for all models. The level of accuracy is similar to that of the correlation function found in figure 4, matching the data all the way down to $r = 20 \text{ Mpc } h^{-1}$.

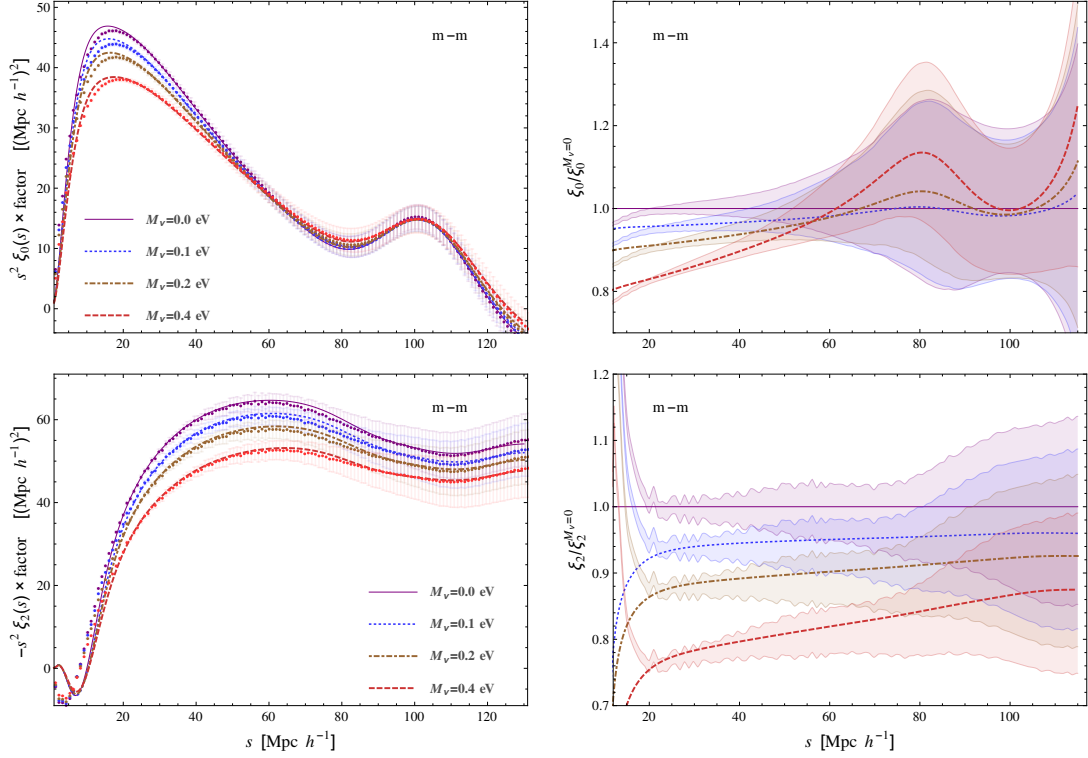


Figure 6. Total matter ($m = cb + \nu$ particles) redshift space correlation functions. The upper figures show the monopole and the lower figures the quadrupole. The right panels show the ratios over the massless case, with the shaded regions the simulated data errors. We use EFT parameters $\alpha_\sigma \times f_0^2 / (\text{Mpc } h^{-1})^2 = 13.5, 15.5, 16, 17.5$ for $M_\nu = 0.0, 0.1, 0.2, 0.4$ eV, respectively.

To compare to the total matter simulated data we proceed in an analogous way as we did for the real space correlation function. We substitute PL_{cb}^L by P_m^L in the leading order functions entering eqs. (6.13) and (6.14), and multiply by f_{cb}^2 the loop contributions. The comparisons among the theory and simulations are shown in figure 6. The top panels show the monopole of the redshift space correlation function and the bottom panels their quadrupole. We have used EFT parameters, reported in $\text{Mpc}^2 h^{-2}$ units, $\alpha_\sigma = 13.5/f_0^2$ for the massless neutrinos, $\alpha_\sigma = 15.5/f_0^2$ for $M_\nu = 0.1$ eV, $\alpha_\sigma = 16/f_0^2$ for $M_\nu = 0.2$ eV, and $\alpha_\sigma = 17.5/f_0^2$ for $M_\nu = 0.4$ eV.

7 Results for halos

We will now compare our theory for redshift and real space correlation functions to halos obtained from the QUIJOTE simulations. The simulation halos are identified using a Friends-of-friends algorithm [66] run on the CDM particles only, with linking length parameter $b = 0.2$. The halo mass, therefore is just a sum over the masses of all particles that are associated with an individual halo. Here, we consider halos with masses in the range $10^{13.1} M_\odot h^{-1} < M_h < 10^{13.5} M_\odot h^{-1}$.

Each model we test has four free parameters, three biases b_1, b_2 and $b_{\nabla^2 \delta}$ and one EFT parameter α_σ , that we adjust empirically to fit three simulated data sets: the real space

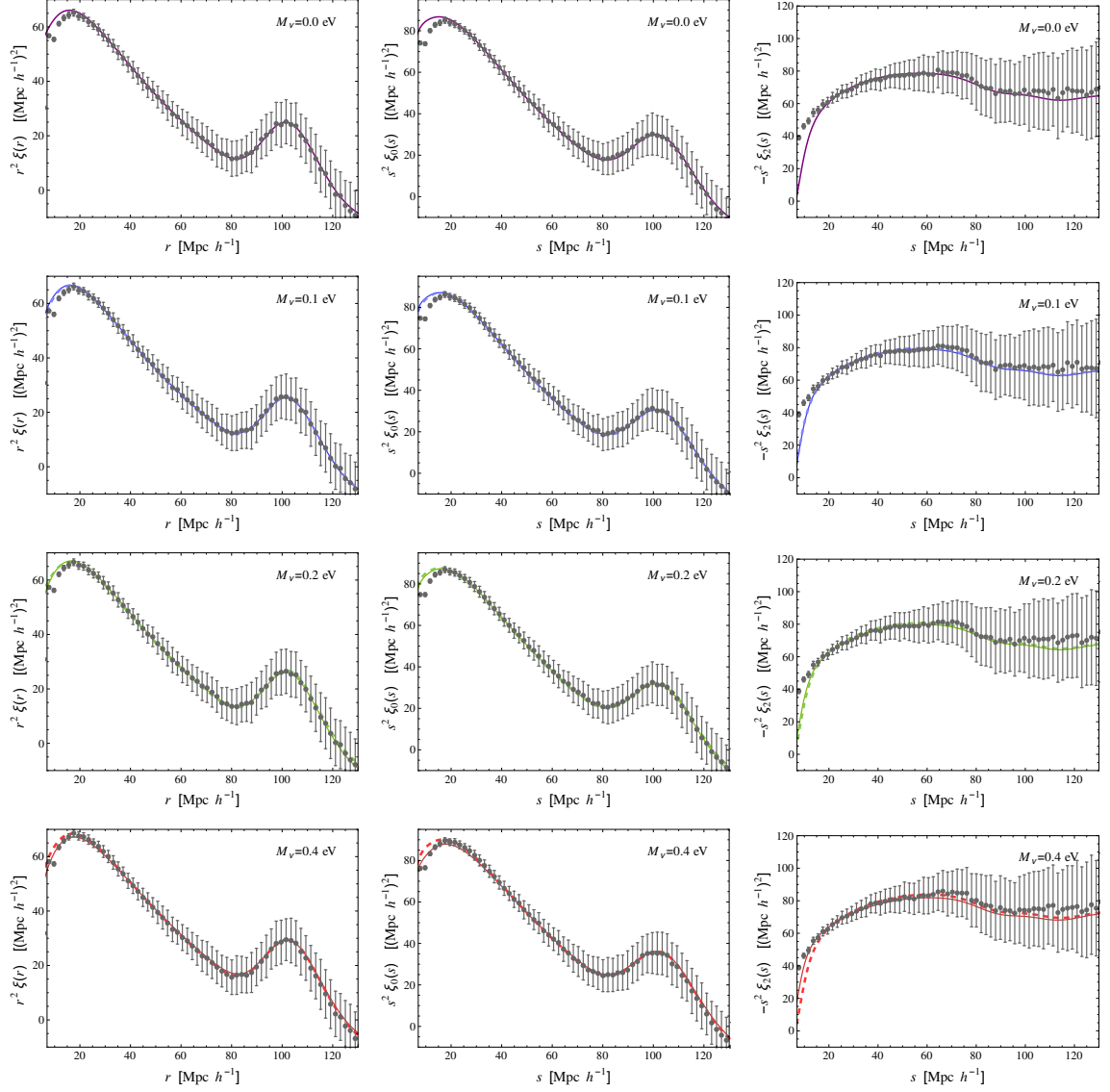


Figure 7. Halo correlation functions in real space (left column) and $\ell = 0, 2$ multipoles in redshift space (middle and right columns, respectively). From top to bottom we show the cases $M_\nu = 0, 0.1, 0.2, 0.4$ eV. The solid lines are obtained by applying the biasing scheme to the cb fluid and the dashed lines to the total matter $m = cb + \nu$. The bias parameters are given in table 1. The relative errors with the simulated data are shown in figure 8.

correlation function, and the $\ell = 0, 2$ multipoles of the redshift-space correlation function. We do this for both biasing the cb and m correlation functions. However, since the real space correlation function is not available to real surveys, we only use it (for simplicity) to fit to the overall large-scale shift given by b_1 , and the other three free parameters are estimated by fitting to redshift-space data directly.

In the presence of massive neutrinos, even linear bias is scale-dependent. In [43, 46], it

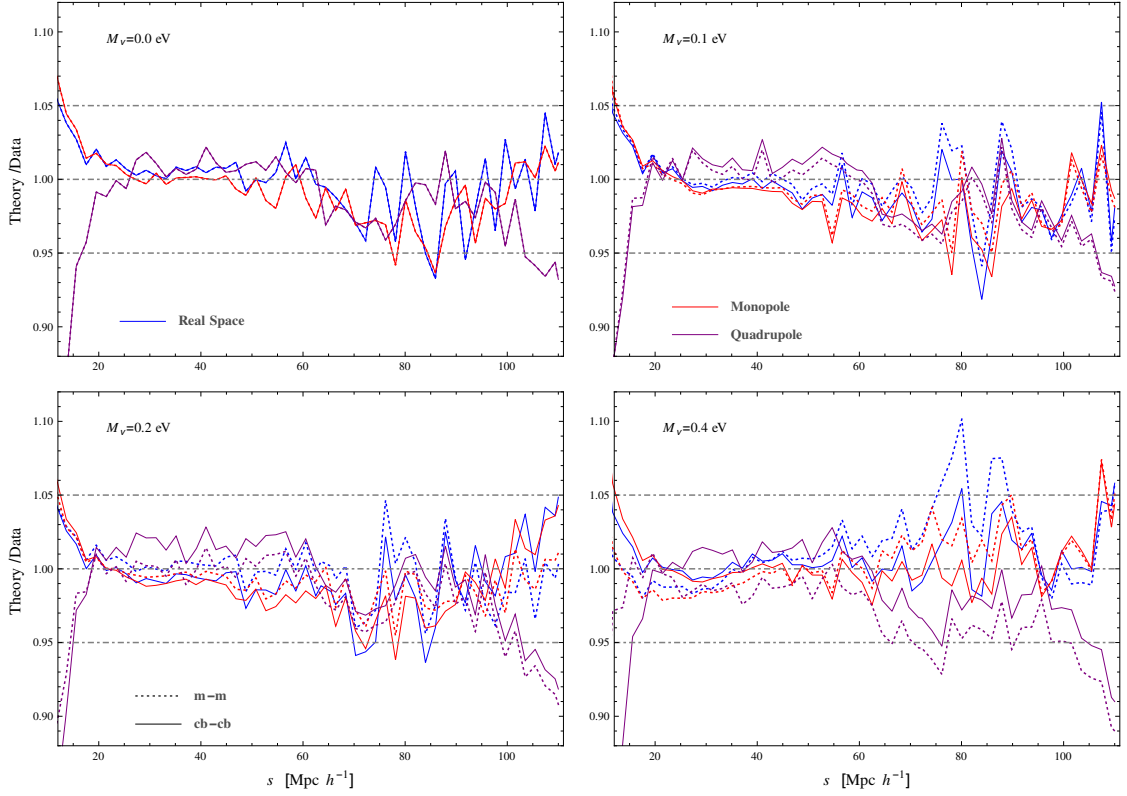


Figure 8. Ratios of halo correlation functions to simulated data. The different panels show the cases of neutrinos with masses $M_\nu = 0, 0.1, 0.2, 0.4$ eV. Solid lines correspond to the biasing scheme applied to the cb fluid and dotted lines to the whole matter fluid. Blue lines are for the real space correlation function, red lines for the redshift space monopole and purple lines for the quadrupole.

is found that

$$b_{\text{LS}}(k) = b_c + b_\nu \frac{P_{cb,\nu}(k)}{P_{cb,cb}(k)} \quad (7.1)$$

is a good approximation for linear bias being the effect of b_ν more pronounced when biasing the m field, and almost negligible when biasing the cb field, because dark matter halos are biased tracers almost entirely of the cb field [42]. Here, we will expand the ratio of power spectra in powers of k^2/k_{FS}^2 , and obtain an effective bias at large scales

$$b_{\text{LS}}(k) = 1 + b_1 - b_{\nabla^2\delta} k^2 + \dots \quad (7.2)$$

That is, we encapsulate the effects of the scale dependent bias as higher-order, curvature biases. This is the main reason why we included it in sections 5 and 6. However, curvature bias serves also to remove large-scale dependencies arising when smoothing the density perturbations [60, 67]; and furthermore, it is degenerate with counterterms to zero-lag, 2-point correlators of linear Lagrangian displacements [41, 61]. Hence, these three effects contribute to the estimated value of $b_{\nabla^2\delta}$. Nonetheless, we shall try to keep $b_{\nabla^2\delta}$ consistent with zero as much as possible when biasing the cb field.

Note however that the expansion of the scale-dependent linear bias in powers of k^2 of eq. (7.2) is formally valid above the free-streaming scale, that may be large. For our

	b_1	b_2	$b_{\nabla^2\delta}$	$\alpha_\sigma \times f_0^2$
(m-m)				
$M_\nu = 0.0$ eV	0.725	-0.1	0	-7
$M_\nu = 0.1$ eV	0.715	-0.2	1	-10
$M_\nu = 0.2$ eV	0.705	-0.3	1	-12
$M_\nu = 0.4$ eV	0.67	-0.5	1	-18
(cb-cb)				
$M_\nu = 0.1$ eV	0.7	-0.4	0	-14
$M_\nu = 0.2$ eV	0.69	-0.1	0	-10
$M_\nu = 0.4$ eV	0.665	-0.2	0.5	-10

Table 1. Lagrangian bias parameters. The top panel shows the parameters when biasing the total matter field, and the lower panel the cb field. The units of parameters $b_{\nabla^2\delta}$ and α_σ are $\text{Mpc}^2 h^{-2}$.

cosmology at $z = 0.5$, this becomes $1/k_{\text{FS}} \approx 70 \text{ Mpc } h^{-1}$ for degenerated neutrinos with total mass $M_\nu = 0.1$ eV; for more massive neutrinos, the free streaming scale is smaller. In spite of this, we show below that curvature bias provides a good match to the simulated halos, better than if not considered.

Our results are shown in figure 7, where we present the correlation functions for the different models, multiplied by factors r^2 to cover the whole range of interest. From top to bottom the panels show the cases $M_\nu = 0, 0.1, 0.2, 0.4$ eV. The left column is for the real space correlation function, the middle column for the redshift-space monopole, and the right column for the redshift-space quadrupole. The points denote the average of the 100 different realizations of the simulated data and the error bars capture their scatter. The solid lines are the results of our theory when biasing the cb field, and the dashed lines when biasing the m field. Figure 8 shows the ratios of the LPT predictions to the N -body data points, with blue lines showing the real space correlation function, red lines the monopole, and purple lines the quadrupole; dashed lines are for the m field and solid lines for the cb field. The bias and EFT parameters of these fittings are shown in table 1. We notice that the more commonly used, Eulerian linear bias is related to the linear local Lagrangian bias as $b_1^E = 1 + b_1$, hence the biases for the different models are very close to each other, and are slightly smaller for more massive neutrinos. This is a consequence of the almost universal halo mass function for cosmologies that have the same σ_8 [42]. All our theoretical results are consistent with the simulations inside the RMS errors down to $r = 20 \text{ Mpc } h^{-1}$. However, the errors are large, so we performed the fittings trying to match as much as possible the points pondering the large scales, but maintaining a good match inside the error bars at scales $20 \text{ Mpc } h^{-1}$. When we compare between the different models, we note that the $M_\nu = 0.4$ eV case performs worse than the other cases, particularly when considering biasing with respect to the total matter field (dashed lines of fig. 8). The bias parameters are degenerate to some extent, especially b_2 and α_σ for the quadrupole. Hence, different combinations of parameters give similar results, here we report those that seem to match the best. However, we found better fits to the

$M_\nu = 0.4$ eV case by using a negative curvature bias $b_{\nabla^2\delta} = -2 \text{ Mpc}^2 h^{-2}$ and a large (also negative) second order local bias $b_2 = -1$. But this is unappealing since eqs. (7.1) and (7.2) suggest curvature bias should be positive; moreover, a negative curvature bias translates into a positive contribution $k^2 P_L(k)$ to the 1-loop power spectrum.

8 Summary and Conclusions

In this work we have developed a PT framework to study the clustering of matter and tracers in cosmologies that contain massive neutrinos. A main complication in constructing such theories is that the large neutrino thermal velocities inhibit formation of structures below the free-streaming scale. This implies that the linear growth becomes suppressed at scales below it, but behaves similar to a CDM-only Universe at larger scales. This scale-dependent growth is inherited to higher orders in PT, modifying the commonly used EdS kernel for both Eulerian and Lagrangian treatments. The latter is the subject of this work.

Our Lagrangian theory is presented in Section 2, arriving to the evolution equation for the Lagrangian displacements in eq. (2.24), where the “additional” free-streaming scale enters through the function $A(k)$. In constructing the theory we make use of non-linear mappings of Fourier transforms of functions evaluated on Eulerian coordinates to Fourier transforms of the same functions evaluated at Lagrangian positions. These maps between Eulerian and Lagrangian frames have a geometrical origin and introduce new terms into the perturbative expansions, ultimately leading to the last two contributions of eq. (2.24), that we refer throughout as “frame-lagging”, following [48]. We obtain the Lagrangian displacements kernels up to third order in PT, which are given by eqs. (3.4), (3.8) and (3.18). These reduce to the well known EdS kernels for massless neutrinos, as can be shown by simply setting the function $A(k) = 3H^2/2$, and the frame-lagging kernels to zero. However, taking the large scale limit to the LPT kernels show a correct behavior only when the frame-lagging contributions are accounted for, since these provide the precise cancellations to reduce the non-linear Lagrangian displacements to those of a pure CDM fluid. Moreover, the second and third order kernels contracted with external wavevectors behave as $k^i L_i \propto k^2$ for $k \ll k_{\text{FS}}$.

Note that we do not treat neutrinos and CDM on an equal footing. Instead, we choose the Lagrangian displacements to follow the trajectories of the CDM particles only, while non-linear neutrinos are modeled as being proportional to the CDM non-linear fluctuations damped by a factor given by the ratio of linear neutrino to CDM overdensities; this is similar to what is done in some PT treatments posed in the Eulerian frame [13, 15]. We show that the above mentioned approximation for the neutrino overdensities does not yield to UV divergences in loop statistics, as ref. [17] claims happens in the Eulerian treatment. In our approach the approximation receives contributions from non-linear Lagrangian displacements as given in eq. (4.3), ensuring a good convergence at large-scales. To show more clearly the importance of the frame-lagging, we use the LPT kernels to construct the SPT real space power spectrum, and show that the loop contributions are free of unwanted UV divergences and behave as $k^2 P_L(k)$ for $k \rightarrow 0$, such that the large scales properly decouple from the small scales. This is not the case if we do not consider the frame-lagging; instead, in that case, the large-scales receive arbitrary, cut-off dependent contributions from the small scales. This small scale sensitivity is a common feature of methods that breaks Galilean invariance or momentum conservation is violated, as in perturbative schemes that approximate the neutrino density by its linear value.

We use our LPT to construct real and redshift space correlation functions for particles and tracers, using standard tools of CLPT and the Gaussian Streaming Model, with small modifications to account for kernels beyond EdS, already found in previous works [39, 50]. (Although those works focus on Modified Gravity theories, the expressions for 2-point statistics are valid for general LPT kernels.) We compare our analytical results to the QUIJOTE suite of simulations finding a good match inside error bars down to $20 \text{ Mpc } h^{-1}$ to the real space and redshift monopole correlation functions of both matter and cb particles with no free parameters. The same accuracy is obtained for the redshift-space quadrupole if we include an EFT parameter, as noted in earlier works on the GSM. For halos, we use a simple Lagrangian biasing prescription that includes only density and curvature operators, we found that this is sufficient to obtain a good agreement to our simulated halos down to $20 \text{ Mpc } h^{-1}$ inside the error bars. More complicated biasing schemes can be incorporated if necessary, for example to include tidal bias; as done in [41] for the GSM. Our comparisons were performed for biasing the cb fluid and the whole matter fluid, for degenerated massive neutrinos with total mass $M_\nu = 0, 0.1, 0.2, 0.4 \text{ eV}$, all showing the same level of accuracy inside the error bars. When comparing to halos we notice that the curvature bias is consistent with zero when the biasing is performed to the cb densities, but not to the $cb + \nu$ fluid. This is not surprising, since early works have shown that the linear bias is almost scale-independent for the former case, but not for the latter.

To our knowledge this work presents the first consistent LPT for CDM clustering in the presence of massive neutrinos.¹¹ Moreover, this is the first analytical, PT method that accounts for both the effects of RSD and non-linear bias for cosmologies with massive neutrinos. Hence, a natural next step is to map our LPT to SPT kernels to obtain the RSD multipoles for the power spectrum. Other interesting avenue of study is the analytical construction of marked statistics that up-weights low density regions, as was done in [68, 69] for MG theories, and that recently have been shown to be promising tools for measuring the absolute mass of the neutrinos with surveys data [70, 71].

This work also has implications for generating consistent initial conditions for N -body simulations in massive neutrino cosmologies with higher order perturbation theory. In Λ CDM cosmologies, initial conditions are routinely generated using second order Lagrangian Perturbation theory [72]. Apart from greater accuracy, use of 2LPT also allows for the simulations to be started later, thereby saving valuable computational time. On the other hand, N -body simulations with massive neutrinos are generally initialized using the first order Zeldovich Approximation, and therefore need to start at higher redshifts for the same level of accuracy. This can also lead to systematic issues when comparing results from simulations with and without massive neutrinos. A consistent 2LPT framework in massive neutrino cosmologies alleviates these issues, and building a framework for initializing massive neutrino cosmology simulations with 2LPT initial conditions provides a particularly appealing application of the results derived in this work.

Acknowledgments

We would like to thank Emanuele Castorina, Jorge L. Cervantes-Cota, Martin White and Francisco Villaescusa-Navarro for discussions and suggestions. A.A. acknowledges partial support from Conacyt Grant No. 283151. A.A. acknowledges the KIPAC-PAVES (Program

¹¹In ref. [22] the degradation and shift of the BAO peak of the real space correlation function is studied within the Lagrangian resummation theory of [23] with the use of EdS kernels.

for Astrophysics Visitor Exchange at Stanford) project. AB would like to thank Stanford University and the Stanford Research Computing Center for providing computational resources and support that contributed to these research results. The PYLIANS3¹² analysis library was used extensively in this paper.

A k - and q -functions

In this appendix we show how the functions A , U and W appear in the real space correlation function, the pairwise velocity and the pairwise velocity dispersion are reduced to expressions suitable for numerical integration. We will refer the reader to [48, 50], and specially to appendix A of [39] where all these functions are displayed. These articles focus on MG models, but the expressions are valid for generalized kernels.

We take as example the function $\dot{A}_{ij}(\mathbf{q})$, for which we have

$$\dot{A}_{ij}(\mathbf{q}) = \langle \Delta_i \frac{\dot{\Delta}_j}{f_0 H} \rangle = \int \frac{d^3 k_1}{(2\pi)^3} \frac{d^3 k_2}{(2\pi)^3} (e^{i\mathbf{k}_1 \cdot \mathbf{q}_2} - e^{i\mathbf{k}_1 \cdot \mathbf{q}_1}) (e^{i\mathbf{k}_2 \cdot \mathbf{q}_2} - e^{i\mathbf{k}_2 \cdot \mathbf{q}_1}) \langle \Psi_i(\mathbf{k}_1) \frac{\dot{\Psi}_i(\mathbf{k}_2)}{f_0 H} \rangle. \quad (\text{A.1})$$

Rotational symmetry and homogeneity imply there are two $|\mathbf{k}|$ -dependent functions, $a(k)$ and $p(k)$, such that

$$\langle \Psi_i(\mathbf{k}) \frac{\dot{\Psi}_i(\mathbf{k}')}{f_0 H} \rangle = (2\pi)^3 \delta_{\text{D}}(\mathbf{k} + \mathbf{k}') \left(a(k) \delta_{ij} + p(k) \frac{k_i k_j}{k^2} \right) = (2\pi)^3 \delta_{\text{D}}(\mathbf{k} + \mathbf{k}') p(k) \frac{k_i k_j}{k^2}, \quad (\text{A.2})$$

where in the last equality we have used the assumption that the Lagrangian displacement is longitudinal, $\Psi_i(\mathbf{k}) = (\hat{k}_j \Psi_j) \hat{k}_i$. Hence

$$\dot{A}_{ij}(\mathbf{q}) = 2 \int \frac{d^3 k}{(2\pi)^3} (1 - e^{i\mathbf{k} \cdot \mathbf{q}}) \frac{k_i k_j}{k^2} p(k). \quad (\text{A.3})$$

Then, we expand the Lagrangian displacement and its derivative as $\Psi = \Psi^{(1)} + \Psi^{(2)} + \dots$ and $\dot{\Psi} = \dot{\Psi}^{(1)} + \dot{\Psi}^{(2)} + \dots$, and obtain that function $p(k)$ is

$$p(k) = \frac{f(k)}{f_0} P_{cb}^L(k) + \frac{9}{49} Q_1^f(k) + \frac{5}{21} \frac{f(k)}{f_0} R_1(k) + \frac{5}{7} R_1^f(k), \quad (\text{A.4})$$

with functions

$$Q_1(k) = \int \frac{d^3 p}{(2\pi)^3} [\Gamma_2(\mathbf{k} - \mathbf{p}, \mathbf{p})]^2 P_{cb}^L(|\mathbf{k} - \mathbf{p}|) P_{cb}^L(p), \quad (\text{A.5})$$

$$Q_1^f(k) = \int \frac{d^3 p}{(2\pi)^3} \Gamma_2(\mathbf{k} - \mathbf{p}, \mathbf{p}) \Gamma_2^f(\mathbf{k} - \mathbf{p}, \mathbf{p}) P_{cb}^L(|\mathbf{k} - \mathbf{p}|) P_{cb}^L(p), \quad (\text{A.6})$$

$$R_1(k) = \int \frac{d^3 p}{(2\pi)^3} \frac{21}{10} C_3 \Gamma_3(\mathbf{k}, -\mathbf{p}, \mathbf{p}) P_{cb}^L(k) P_{cb}^L(p), \quad (\text{A.7})$$

$$R_1^f(k) = \int \frac{d^3 p}{(2\pi)^3} \frac{21}{10} C_3 \Gamma_3^f(\mathbf{k}, -\mathbf{p}, \mathbf{p}) P_{cb}^L(k) P_{cb}^L(p). \quad (\text{A.8})$$

¹²<https://github.com/franciscovillaescusa/Pylians3>

We have used the “scalar” kernels for $k_i\Psi_i$ and $k_i\dot{\Psi}_i$, given by [39]

$$C_n\Gamma_n(\mathbf{k}_1, \dots, \mathbf{k}_n; t) = k_{1\dots n}^i L_i^{(n)}(\mathbf{k}_1 \dots, \mathbf{k}_n; t) \quad (\text{A.9})$$

$$C_n\Gamma_n^f(\mathbf{k}_1, \dots, \mathbf{k}_n; t) = k_{1\dots n}^i L_i^{f(n)}(\mathbf{k}_1 \dots, \mathbf{k}_n; t), \quad (\text{A.10})$$

where we choose $C_1 = 1$ and $C_2 = 3/7$. The first order scalar kernels are $\Gamma_1(\mathbf{k}) = 1$ and $\Gamma_1^f(\mathbf{k}) = f(k)/f_0$. To second order

$$\Gamma_2(\mathbf{p}_1, \mathbf{p}_2) = \left[\mathcal{A} - \mathcal{B} \frac{(\mathbf{p}_1 \cdot \mathbf{p}_2)^2}{p_1^2 p_2^2} \right] = \frac{7}{3} \frac{D^{(2)}(\mathbf{p}_1, \mathbf{p}_2)}{D_+(p_1)D_+(p_2)}, \quad (\text{A.11})$$

$$\begin{aligned} \Gamma_2^f(\mathbf{p}_1, \mathbf{p}_2) &= \Gamma_2(\mathbf{p}_1, \mathbf{p}_2) \frac{f(p_1) + f(p_2)}{2f_0} + \frac{1}{2f_0 H_0} \left[\dot{\mathcal{A}} - \dot{\mathcal{B}} \frac{(\mathbf{p}_1 \cdot \mathbf{p}_2)^2}{p_1^2 p_2^2} \right], \\ &= \frac{1}{2f_0 H} \frac{7}{3} \frac{\frac{d}{dt} D^{(2)}(\mathbf{p}_1, \mathbf{p}_2)}{D_+(p_1)D_+(p_2)}, \end{aligned} \quad (\text{A.12})$$

where $\mathcal{A}, \mathcal{B} = \mathcal{A}, \mathcal{B}(\mathbf{p}_1, \mathbf{p}_2)$. The third order scalar kernels are

$$C_3\Gamma_3(\mathbf{p}_1, \mathbf{p}_2, \mathbf{p}_3) = \frac{D_+^{(3)s}(\mathbf{p}_1, \mathbf{p}_2, \mathbf{p}_3)}{D_+(\mathbf{p}_1)D_+(\mathbf{p}_2)D_+(\mathbf{p}_3)}, \quad (\text{A.13})$$

$$C_3\Gamma_3^f(\mathbf{p}_1, \mathbf{p}_2, \mathbf{p}_3) = \frac{1}{3f_0 H} \frac{\frac{d}{dt} D_+^{(3)s}(\mathbf{p}_1, \mathbf{p}_2, \mathbf{p}_3)}{D_+(\mathbf{p}_1)D_+(\mathbf{p}_2)D_+(\mathbf{p}_3)}. \quad (\text{A.14})$$

Now, with the solid angle integral identity

$$\frac{1}{4\pi} \int d\Omega_{\hat{\mathbf{k}}} e^{i\mathbf{k} \cdot \mathbf{q}} \hat{k}_i \hat{k}_j = \frac{j_1(kq)}{kq} \delta_{ij} - j_2(kq) \hat{q}_i \hat{q}_j \quad (\text{A.15})$$

we can bring eq. (A.3) to

$$\dot{A}_{ij}(\mathbf{q}) = \dot{X}(q) \delta_{ij} + \dot{Y}(q) \hat{q}_i \hat{q}_j, \quad (\text{A.16})$$

with

$$\dot{X}(q) = \frac{1}{\pi^2} \int dk p(k) \left[\frac{1}{3} - \frac{j_1(kq)}{kq} \right], \quad (\text{A.17})$$

$$\dot{Y}(q) = \frac{1}{\pi^2} \int dk p(k) j_2(kq). \quad (\text{A.18})$$

We notice that for the massless neutrino case, the scalar kernels reduce to

$$\Gamma_n^f \simeq \Gamma_n, \quad (M_\nu = 0), \quad (\text{A.19})$$

which further implies that functions Q^f and R^f reduce to Q and R , and $\dot{A}_{ij}(\mathbf{q})$ to the standard result in Λ CDM (see [38]).

Using the same methods presented here, one can obtain all the “undotted” and “dotted” functions A , W and U , necessary to construct the correlation functions in CLPT and the GSM. All these functions are displayed in appendix A of ref. [39], which are valid for general kernels Γ and Γ^f . In that reference one can find also how to introduce tidal bias into the GSM for generalized LPT kernels.

References

- [1] I. Esteban, M. Gonzalez-Garcia, A. Hernandez-Cabezudo, M. Maltoni and T. Schwetz, *Global analysis of three-flavour neutrino oscillations: synergies and tensions in the determination of θ_{23} , δ_{CP} , and the mass ordering*, *JHEP* **01** (2019) 106, [[1811.05487](#)].
- [2] PLANCK collaboration, N. Aghanim et al., *Planck 2018 results. VI. Cosmological parameters*, [1807.06209](#).
- [3] J. Lesgourgues and S. Pastor, *Massive neutrinos and cosmology*, *Phys. Rept.* **429** (2006) 307–379, [[astro-ph/0603494](#)].
- [4] W. Hu, D. J. Eisenstein and M. Tegmark, *Weighing neutrinos with galaxy surveys*, *Phys. Rev. Lett.* **80** (1998) 5255–5258, [[astro-ph/9712057](#)].
- [5] LSST Science Collaboration, P. A. Abell, J. Allison, S. F. Anderson, J. R. Andrew, J. R. P. Angel et al., *LSST Science Book, Version 2.0*, *arXiv e-prints* (Dec., 2009) arXiv:0912.0201, [[0912.0201](#)].
- [6] A. Font-Ribera, P. McDonald, N. Mostek, B. A. Reid, H.-J. Seo and A. Slosar, *DESI and other dark energy experiments in the era of neutrino mass measurements*, *JCAP* **05** (2014) 023, [[1308.4164](#)].
- [7] B. Audren, J. Lesgourgues, S. Bird, M. G. Haehnelt and M. Viel, *Neutrino masses and cosmological parameters from a Euclid-like survey: Markov Chain Monte Carlo forecasts including theoretical errors*, *JCAP* **2013** (Jan., 2013) 026, [[1210.2194](#)].
- [8] S. Hannestad and T. Schwetz, *Cosmology and the neutrino mass ordering*, *JCAP* **11** (2016) 035, [[1606.04691](#)].
- [9] F. Bernardeau, S. Colombi, E. Gaztanaga and R. Scoccimarro, *Large scale structure of the universe and cosmological perturbation theory*, *Phys. Rept.* **367** (2002) 1–248, [[astro-ph/0112551](#)].
- [10] S. Saito, M. Takada and A. Taruya, *Impact of massive neutrinos on nonlinear matter power spectrum*, *Phys. Rev. Lett.* **100** (2008) 191301, [[0801.0607](#)].
- [11] Y. Y. Y. Wong, *Higher order corrections to the large scale matter power spectrum in the presence of massive neutrinos*, *JCAP* **0810** (2008) 035, [[0809.0693](#)].
- [12] S. Saito, M. Takada and A. Taruya, *Nonlinear power spectrum in the presence of massive neutrinos: perturbation theory approach, galaxy bias and parameter forecasts*, *Phys. Rev.* **D80** (2009) 083528, [[0907.2922](#)].
- [13] J. Lesgourgues, S. Matarrese, M. Pietroni and A. Riotto, *Non-linear Power Spectrum including Massive Neutrinos: the Time-RG Flow Approach*, *JCAP* **0906** (2009) 017, [[0901.4550](#)].
- [14] M. Shoji and E. Komatsu, *Third-order Perturbation Theory With Non-linear Pressure*, *Astrophys. J.* **700** (2009) 705–719, [[0903.2669](#)].
- [15] A. Upadhye, R. Biswas, A. Pope, K. Heitmann, S. Habib, H. Finkel et al., *Large-Scale Structure Formation with Massive Neutrinos and Dynamical Dark Energy*, *Phys. Rev.* **D89** (2014) 103515, [[1309.5872](#)].
- [16] H. Dupuy and F. Bernardeau, *Describing massive neutrinos in cosmology as a collection of independent flows*, *JCAP* **01** (2014) 030, [[1311.5487](#)].
- [17] D. Blas, M. Garny, T. Konstandin and J. Lesgourgues, *Structure formation with massive neutrinos: going beyond linear theory*, *JCAP* **1411** (2014) 039, [[1408.2995](#)].
- [18] F. F  hrer and Y. Y. Y. Wong, *Higher-order massive neutrino perturbations in large-scale structure*, *JCAP* **03** (2015) 046, [[1412.2764](#)].

- [19] E. Castorina, C. Carbone, J. Bel, E. Sefusatti and K. Dolag, *DEMNUi: The clustering of large-scale structures in the presence of massive neutrinos*, *JCAP* **07** (2015) 043, [[1505.07148](#)].
- [20] M. Levi and Z. Vlah, *Massive neutrinos in nonlinear large scale structure: A consistent perturbation theory*, [1605.09417](#).
- [21] L. Senatore and M. Zaldarriaga, *The Effective Field Theory of Large-Scale Structure in the presence of Massive Neutrinos*, [1707.04698](#).
- [22] M. Peloso, M. Pietroni, M. Viel and F. Villaescusa-Navarro, *The effect of massive neutrinos on the BAO peak*, *JCAP* **07** (2015) 001, [[1505.07477](#)].
- [23] T. Matsubara, *Resumming Cosmological Perturbations via the Lagrangian Picture: One-loop Results in Real Space and in Redshift Space*, *Phys. Rev. D* **77** (2008) 063530, [[0711.2521](#)].
- [24] B. S. Wright, H. A. Winther and K. Koyama, *COLA with massive neutrinos*, *JCAP* **10** (2017) 054, [[1705.08165](#)].
- [25] J. Brandbyge and S. Hannestad, *Grid based linear neutrino perturbations in cosmological n-body simulations*, *Journal of Cosmology and Astroparticle Physics* **2009** (May, 2009) 002–002.
- [26] M. Viel, M. G. Haehnelt and V. Springel, *The effect of neutrinos on the matter distribution as probed by the intergalactic medium*, *Journal of Cosmology and Astroparticle Physics* **2010** (Jun, 2010) 015–015.
- [27] Y. Ali-Haïmoud and S. Bird, *An efficient implementation of massive neutrinos in non-linear structure formation simulations*, *Monthly Notices of the Royal Astronomical Society* **428** (Nov, 2012) 3375–3389.
- [28] A. Banerjee and N. Dalal, *Simulating nonlinear cosmological structure formation with massive neutrinos*, *JCAP* **11** (2016) 015, [[1606.06167](#)].
- [29] D. Inman and U.-L. Pen, *Cosmic neutrinos: A dispersive and nonlinear fluid*, *Physical Review D* **95** (Mar, 2017) .
- [30] A. Banerjee, D. Powell, T. Abel and F. Villaescusa-Navarro, *Reducing noise in cosmological n-body simulations with neutrinos*, *Journal of Cosmology and Astroparticle Physics* **2018** (Sep, 2018) 028–028.
- [31] S. Bird, Y. Ali-Haïmoud, Y. Feng and J. Liu, *An efficient and accurate hybrid method for simulating non-linear neutrino structure*, *Monthly Notices of the Royal Astronomical Society* **481** (08, 2018) 1486–1500, [<https://academic.oup.com/mnras/article-pdf/481/2/1486/25716087/sty2376.pdf>].
- [32] J. Dakin, J. Brandbyge, S. Hannestad, T. Haugbølle and T. Tram, *ν concept: cosmological neutrino simulations from the non-linear boltzmann hierarchy*, *Journal of Cosmology and Astroparticle Physics* **2019** (Feb, 2019) 052–052.
- [33] M. Shoji and E. Komatsu, *Massive Neutrinos in Cosmology: Analytic Solutions and Fluid Approximation*, *Phys. Rev. D* **81** (2010) 123516, [[1003.0942](#)].
- [34] A. Aviles, *Dark matter dispersion tensor in perturbation theory*, *Phys. Rev. D* **93** (2016) 063517, [[1512.07198](#)].
- [35] G. Cusin, V. Tansella and R. Durrer, *Vorticity generation in the Universe: A perturbative approach*, *Phys. Rev. D* **95** (2017) 063527, [[1612.00783](#)].
- [36] J. Carlson, B. Reid and M. White, *Convolution Lagrangian perturbation theory for biased tracers*, *Mon. Not. Roy. Astron. Soc.* **429** (2013) 1674, [[1209.0780](#)].
- [37] B. A. Reid and M. White, *Towards an accurate model of the redshift space clustering of halos in the quasilinear regime*, *Mon. Not. Roy. Astron. Soc.* **417** (2011) 1913–1927, [[1105.4165](#)].
- [38] L. Wang, B. Reid and M. White, *An analytic model for redshift-space distortions*, *Mon. Not. Roy. Astron. Soc.* **437** (2014) 588–599, [[1306.1804](#)].

- [39] G. Valogiannis, R. Bean and A. Aviles, *An accurate perturbative approach to redshift space clustering of biased tracers in modified gravity*, *JCAP* **2001** (2020) 055, [[1909.05261](#)].
- [40] F. Villaescusa-Navarro et al., *The Quijote simulations*, [1909.05273](#).
- [41] Z. Vlah, E. Castorina and M. White, *The Gaussian streaming model and convolution Lagrangian effective field theory*, *JCAP* **12** (2016) 007, [[1609.02908](#)].
- [42] F. Villaescusa-Navarro, F. Marulli, M. Viel, E. Branchini, E. Castorina, E. Sefusatti et al., *Cosmology with massive neutrinos I: towards a realistic modeling of the relation between matter, haloes and galaxies*, *JCAP* **03** (2014) 011, [[1311.0866](#)].
- [43] E. Castorina, E. Sefusatti, R. K. Sheth, F. Villaescusa-Navarro and M. Viel, *Cosmology with massive neutrinos II: on the universality of the halo mass function and bias*, *JCAP* **02** (2014) 049, [[1311.1212](#)].
- [44] M. LoVerde, *Halo bias in mixed dark matter cosmologies*, *Phys. Rev. D* **90** (2014) 083530, [[1405.4855](#)].
- [45] S. Vagnozzi, T. Brinckmann, M. Archidiacono, K. Freese, M. Gerbino, J. Lesgourgues et al., *Bias due to neutrinos must not uncorrect'd go*, *JCAP* **09** (2018) 001, [[1807.04672](#)].
- [46] A. Banerjee, E. Castorina, F. Villaescusa-Navarro, T. Court and M. Viel, *Weighing neutrinos with the halo environment*, [1907.06598](#).
- [47] T. Matsubara, *Recursive Solutions of Lagrangian Perturbation Theory*, *Phys. Rev. D* **92** (2015) 023534, [[1505.01481](#)].
- [48] A. Aviles and J. L. Cervantes-Cota, *Lagrangian perturbation theory for modified gravity*, *Phys. Rev. D* **96** (2017) 123526, [[1705.10719](#)].
- [49] H. A. Winther, K. Koyama, M. Manera, B. S. Wright and G.-B. Zhao, *COLA with scale-dependent growth: applications to screened modified gravity models*, *JCAP* **08** (2017) 006, [[1703.00879](#)].
- [50] A. Aviles, M. A. Rodriguez-Meza, J. De-Santiago and J. L. Cervantes-Cota, *Nonlinear evolution of initially biased tracers in modified gravity*, *JCAP* **1811** (2018) 013, [[1809.07713](#)].
- [51] G. Valogiannis and R. Bean, *Convolution Lagrangian perturbation theory for biased tracers beyond general relativity*, *Phys. Rev. D* **99** (2019) 063526, [[1901.03763](#)].
- [52] C. Moretti, S. Mozzon, P. Monaco, E. Munari and M. Baldi, *Fast numerical method to generate halo catalogues in modified gravity (part I): second-order Lagrangian perturbation theory*, *Mon. Not. Roy. Astron. Soc.* **493** (2020) 1153–1164, [[1909.06282](#)].
- [53] W. Hu and D. J. Eisenstein, *Small scale perturbations in a general MDM cosmology*, *Astrophys. J.* **498** (1998) 497, [[astro-ph/9710216](#)].
- [54] M. McQuinn and M. White, *Cosmological perturbation theory in 1+1 dimensions*, *JCAP* **01** (2016) 043, [[1502.07389](#)].
- [55] T. Matsubara, *Nonlinear Perturbation Theory Integrated with Nonlocal Bias, Redshift-space Distortions, and Primordial Non-Gaussianity*, *Phys. Rev. D* **83** (2011) 083518, [[1102.4619](#)].
- [56] C. Rampf and T. Buchert, *Lagrangian perturbations and the matter bispectrum I: fourth-order model for non-linear clustering*, *JCAP* **06** (2012) 021, [[1203.4260](#)].
- [57] J. J. M. Carrasco, S. Foreman, D. Green and L. Senatore, *The 2-loop matter power spectrum and the IR-safe integrand*, *JCAP* **07** (2014) 056, [[1304.4946](#)].
- [58] A. Lewis, A. Challinor and A. Lasenby, *Efficient computation of CMB anisotropies in closed FRW models*, *Astrophys. J.* **538** (2000) 473–476, [[astro-ph/9911177](#)].
- [59] T. Matsubara, *Nonlinear perturbation theory with halo bias and redshift-space distortions via the Lagrangian picture*, *Phys. Rev. D* **78** (2008) 083519, [[0807.1733](#)].

- [60] A. Aviles, *Renormalization of Lagrangian bias via spectral parameters*, *Phys. Rev. D* **98** (2018) 083541, [[1805.05304](#)].
- [61] Z. Vlah, M. White and A. Aviles, *A Lagrangian effective field theory*, *JCAP* **09** (2015) 014, [[1506.05264](#)].
- [62] C. Uhlemann, M. Kopp and T. Haugg, *Edgeworth streaming model for redshift space distortions*, *Phys. Rev. D* **92** (2015) 063004, [[1503.08837](#)].
- [63] Z. Vlah and M. White, *Exploring redshift-space distortions in large-scale structure*, *JCAP* **1903** (2019) 007, [[1812.02775](#)].
- [64] R. Scoccimarro, *Redshift-space distortions, pairwise velocities and nonlinearities*, *Phys. Rev. D* **70** (2004) 083007, [[astro-ph/0407214](#)].
- [65] K. B. Fisher, *On the validity of the streaming model for the redshift space correlation function in the linear regime*, *Astrophys. J.* **448** (1995) 494–499, [[astro-ph/9412081](#)].
- [66] M. Davis, G. Efstathiou, C. S. Frenk and S. D. M. White, *The evolution of large-scale structure in a universe dominated by cold dark matter*, *ApJ* **292** (May, 1985) 371–394.
- [67] F. Schmidt, D. Jeong and V. Desjacques, *Peak-Background Split, Renormalization, and Galaxy Clustering*, *Phys. Rev. D* **88** (2013) 023515, [[1212.0868](#)].
- [68] M. White, *A marked correlation function for constraining modified gravity models*, *JCAP* **11** (2016) 057, [[1609.08632](#)].
- [69] A. Aviles, K. Koyama, J. L. Cervantes-Cota, H. A. Winther and B. Li, *Marked correlation functions in perturbation theory*, *JCAP* **01** (2020) 006, [[1911.06362](#)].
- [70] E. Massara, F. Villaescusa-Navarro, S. Ho, N. Dalal and D. N. Spergel, *Using the Marked Power Spectrum to Detect the Signature of Neutrinos in Large-Scale Structure*, [2001.11024](#).
- [71] O. H. Philcox, E. Massara and D. N. Spergel, *What does the Marked Power Spectrum Measure? Insights from Perturbation Theory*, [2006.10055](#).
- [72] M. Crocce, S. Pueblas and R. Scoccimarro, *2LPTIC: 2nd-order Lagrangian Perturbation Theory Initial Conditions*, Jan., 2012.